Inorganic Chemistry
Article

Phosphorescent Platinum(II) Complexes Derived from Multifunctional Chromophores: Synthesis, Structures, Photophysics, and Electroluminescence

Ze He,[†] Wai-Yeung Wong,*[,†] Xiaoming Yu,[‡] Hoi-Sing Kwok,[‡] and Zhenyang Lin[§]

Department of Chemistry and Centre for Advanced Luminescence Materials, Hong Kong Baptist University, Waterloo Road, Kowloon Tong, Hong Kong, People's Republic of China, Departments of Electronic and Electrical Engineering and Centre for Display Research and of Chemistry, Hong Kong University of Science and Technology, Clearwater Bay, Hong Kong, People's Republic of China

The synthesis and structural, photophysical, electrochemical, and electroluminescent properties of a novel class of trifunctional Pt(II) cyclometalated complexes are reported in which the hole-transporting triarylamine, electron-transporting oxadiazole, and electroluminescent metal components are integrated into a single molecule. These neutral metal chelates display good thermal stability (>250 °C under N_2) and morphological stability. All of them exhibit intense ligand-centered fluorescence and phosphorescence in fluid solutions at room temperature, but the emission spectra become largely dominated by triplet emission bands in CH_2Cl_2 glass at 77 K. Substituents with different electronic properties were introduced into the bipolar cyclometalating ligands to fine-tune the absorption and emissive characteristics of the compounds, and the results were correlated with theoretical calculations using density functional theory. A comparison of the photophysics and electrochemistry of our multifunctional systems to those only derived from each of the constituent components was also made and discussed. These Pt complexes can be vacuum-sublimed and applied as emissive dopants for the fabrication of vapor-deposited electrophosphorescent organic light-emitting devices (OLEDs), which generally exhibit good device performance with efficiencies up to 3.6%, 11.0 cd A^{-1}, and 5.8 lm W^{-1}. While the electroluminescence energy resembles that recorded in fluid solutions for these Pt emitters, these monochromatic OLEDs can emit tunable colors by varying the aryl ring substituents and the level of doping. Saliently, single dopant white-light electroluminescence, triggered by the simultaneous fluorescence/phosphorescence emission of the metal complexes and a variation of applied driving voltages, has also been realized based on some of these multifunctional complexes with peak electrophosphorescence efficiencies of 6.8 cd A^{-1} and 2.6%.

Introduction

Since the pioneering work by Tang et al. on a multilayer device configuration for small-molecule organic light-emitting diodes (OLEDs),[1] this research field has stimulated tremendous impetus to develop OLEDs using organic or metal−organic compounds as emitters because of its huge market share in next-generation flat-panel display technology.[2] A successful OLED requires facile and balanced charge transport as well as a high conversion efficiency of excitons to light.[3] To fulfill these requirements, OLEDs often contain a number of layers that individually perform the roles of

* To whom correspondence should be addressed. E-mail: rwywong@hkbu.edu.hk.

† Hong Kong Baptist University.

‡ Department of Electronic and Electrical Engineering and Centre for Display Research, Hong Kong University of Science and Technology.

§ Department of Chemistry, Hong Kong University of Science and Technology.

(1) Tang, C. W.; Van Slyke, S. A. *Appl. Phys. Lett.* **1987**, *51*, 913−915.

(2) (a) Chen, C. H.; Shi, J. *Coord. Chem. Rev.* **1998**, *171*, 161−174. (b) Friend, R. H.; Gymer, R. W.; Holmes, A. B.; Burroughes, J. H.; Marks, R. N.; Taliani, C.; Bradley, D. D. C.; Santos, D. A.; Brédas, J. L.; Lögdlund, M.; Salaneck, W. R. *Nature* **1999**, *397*, 121−128. (c) Kraft, A.; Grimsdale, A. C.; Holmes, A. B. *Angew. Chem., Int. Ed.* **1998**, *37*, 402−428. (d) Veinot, J. G. C.; Marks, T. J. *Acc. Chem. Res.* **2005**, *38*, 632−643. (e) Entwistle, C. D.; Marder, T. B. *Angew. Chem., Int. Ed.* **2002**, *41*, 2927−2931. (f) Entwistle, C. D.; Marder, T. B. *Chem. Mater.* **2004**, *16*, 4574−4585.

(3) Hughes, G.; Bryce, M. R. *J. Mater. Chem.* **2005**, *15*, 94−107.

charge transport and light emission.[4] Each layer requires materials with the correct highest occupied molecular orbital (HOMO) and lowest unoccupied molecular orbital (LUMO) energies to either promote or disrupt the flow of charge in the device.[5] The sophisticated multilayer configuration consisting of the hole-transporting (HT), the electron-transporting (ET), and the electroluminescent (EL) layers is frequently used to achieve a balanced injection and transport of holes and electrons. A current challenge for high-efficiency OLEDs is focused on the optimization of device structures[6] and the use of electrophosphorescent OLEDs.[7] Phosphorescent small molecules are promising for achieving highly efficient OLEDs by generation of light emission from both singlet and triplet excitons.[8] Such an impressive approach is to efficiently harvest triplet excitons through incorporation of heavy-metal centers, which would increase spin−orbit coupling to facilitate intersystem crossing into the triplet state. The scope and diversity of studies on metal−organic phosphors in the realm of optoelectronics have continued to expand. Apart from the emission efficiency issue, an exploration of possible methods to bring about a variation in the emission color would also be important. Most of the common approaches involve the use of different light-emitting materials or multicomponent blended mixtures of light emitters with different emission characteristics for color tuning.[9] Remarkably, recent reports have shown that varying emission colors of OLEDs could be generated using metal

phosphors as dopants or nondoping emitters through a change in the dopant concentration or a variation of bias voltages.[10]

Although there is a large body of literature information about electrophosphorescent heavy-metal complexes, utilization of their derivatives playing multifunctional roles for OLEDs was not well elucidated and remains to be largely studied.[11] To our knowledge, only a few trifunctional polymers that rival those from multilayer devices in performance have been prepared.[12] To advance the development of novel metal-based phosphors to fill this gap, we take advantage of the characteristic of Pt d^8 groups coupled with the bipolar character of new charge-balance ligand systems featuring both HT and ET modules. These new neutral complexes can be used not only as emitters but also as multifunctional chromophores for improved charge transportation. Metal-based phosphors composed of a hole-conducting block and an ET unit can combine the properties of both functional components to produce new properties that are hardly possible with either one separately.

Herein, we describe our endeavors to design some electroactive materials composed of simple modular units, each of which performs a specific functional role, namely, electron transfer, hole transfer, and light emission. Furthermore, we chose chromophoric units that may be easily derivatized, thereby giving greater flexibility to this design strategy. This class of Pt complexes is stable with respect to sublimation and thus is suitable for vacuum deposition in small-molecule OLED fabrication. On the other hand, white OLEDs (WOLEDs) have also drawn much attention in the academic and industrial R&D sectors because of their potential use in display backlights, in full color applications, and in solid-state lighting purposes.[13] Interestingly, these new trifunctional Pt(II) cyclometalated complexes, which are capable of emitting strong blue and orange colors in both steady-state emission and electroluminescence, can be exploited in the

(4) Kido, J.; Okamoto, Y. *Chem. Rev.* **2002**, *102*, 2357−2368.

(5) Yersin, H. *Top. Curr. Chem.* **2004**, *242*, 1−42.

(6) (a) Tamoto, N.; Adachi, C.; Nagai, K. *Chem. Mater.* **1997**, *9*, 1077−1085. (b) Mitschke, U.; Bauerle, P. *J. Mater. Chem.* **2000**, *10*, 1471−1507.

(7) (a) Baldo, M. A.; Lamansky, S.; Burrows, P. E.; Thompson, M. E.; Forrest, S. R. *Appl. Phys. Lett.* **1999**, *75*, 4−6. (b) Baldo, M. A.; O'Brien, D. F.; You, Y.; Shoustikov, A.; Sibley, S.; Thompson, M. E.; Forrest, S. R. *Nature* **1998**, *395*, 151−154. (c) Baldo, M. A.; Thompson, M. E.; Forrest, S. R. *Pure Appl. Chem.* **1999**, *71*, 2095−2106. (d) Baldo, M. A.; Thompson, M. E.; Forrest, S. R. *Nature* **2000**, *403*, 750−753. (e) Tsutsui, T.; Yang, M.-J.; Yahiro, M.; Nakamura, K.; Watanabe, T.; Tsuji, T.; Fukuda, Y.; Wakimoto, T.; Miyaguchi, S. *Jpn. J. Appl. Phys.* **1999**, *38*, L1502−L1504. (f) Holder, E.; Langeveld, B. M. W.; Schubert, U. S. *Adv. Mater.* **2005**, *17*, 1109−1121. (g) Li, C.-L.; Su, Y.-J.; Tao, Y.-T.; Chou, P.-T.; Chien, C.-H.; Cheng, C.-C.; Liu, R.-S. *Adv. Funct. Mater.* **2005**, *15*, 387−395. (h) Rayabarapu, D. K.; Paulose, B. M. J. S.; Duan, J.-P.; Cheng, C.-H. *Adv. Mater.* **2005**, *17*, 349−353. (i) Lu, W.; Mi, B.-X.; Chan, M. C. W.; Hui, Z.; Che, C.-M.; Zhu, N.; Lee, S.-T. *J. Am. Chem. Soc.* **2004**, *126*, 4958−4971. (j) Chan, S.-C.; Chan, M. C. W.; Wang, Y.; Che, C.-M.; Cheung, K.-K.; Zhu, N. *Chem.−Eur. J.* **2001**, *7*, 4180−4190. (k) Song, Y.-H.; Yeh, S.-J.; Chen, C.-T.; Chi, Y.; Liu, C.-S.; Yu, J.-K.; Hu, Y.-H.; Chou, P.-T.; Peng, S.-M.; Lee, G.-H. *Adv. Funct. Mater.* **2004**, *14*, 1221−1226. (l) Kavitha, J.; Chang, S.-Y.; Chi, Y.; Yu, J.-K.; Hu, Y.-H.; Chou, P.-T.; Peng, S.-M.; Lee, G.-H.; Tao, Y.-T.; Chien, C.-H.; Carty, A. J. *Adv. Funct. Mater.* **2005**, *15*, 223−229. (m) Tung, Y.-L.; Chen, L.-S.; Chi, Y.; Chou, P.-T.; Cheng, Y.-M.; Li, E. Y.; Lee, G.-H.; Shu, C.-F.; Wu, F.-I.; Carty, A. J. *Adv. Funct. Mater.* **2006**, *16*, 1615−1626. (n) Tung, Y.-L.; Lee, S.-W.; Chi, Y.; Chen, L.-S.; Shu, C.-F.; Wu, F.-I.; Carty, A. J.; Chou, P.-T.; Peng, S.-M.; Lee, G.-H. *Adv. Mater.* **2005**, *17*, 1059−1064. (o) Niu, Y.-H.; Chen, B.; Liu, S.; Yip, H.; Bardecker, J.; Jen, A. K.-Y.; Kavitha, J.; Chi, Y.; Shu, C.-F.; Tseng, Y.-H.; Chien, C.-H. *Appl. Phys. Lett.* **2004**, *85*, 1619−1621. (p) Chang, S.-Y.; Kavitha, J.; Li, S.-W.; Hsu, C.-S.; Chi, Y.; Yeh, Y.-S.; Chou, P.-T.; Lee, G.-H.; Carty, A. J.; Tao, Y.-T.; Chien, C.-H. *Inorg. Chem.* **2006**, *45*, 137−146. (q) Chou, P.-T.; Chi, Y. *Eur. J. Inorg. Chem.* **2006**, 3319−3332.

(8) (a) Köhler, A.; Wilson, J. S.; Friend, R. H. *Adv. Mater.* **2002**, *14*, 701−707. (b) Gong, X.; Robinson, M. R.; Ostrowski, J. C.; Moses, D.; Bazan, G. C.; Heeger, A. J. *Adv. Mater.* **2002**, *14*, 581−585. (c) Adachi, C.; Baldo, M. A.; Thompson, M. E.; Forrest, S. R. *J. Appl. Phys.* **2001**, *90*, 5048−5051.

(9) (a) Kido, J.; Shionoya, H.; Nagai, K. *Appl. Phys. Lett.* **1995**, *67*, 2281−2283. (b) Granstrom, M.; Inganas, O. *Appl. Phys. Lett.* **1996**, *68*, 147−149. (c) Jiang, X.; Zhang, Z.; Zhao, W.; Zhu, W.; Zhang, B.; Zu, S. *J. Phys. D: Appl. Phys.* **2000**, *33*, 473−476. (d) D'Andrade, B. W.; Thompson, M. E.; Forrest, S. R. *Adv. Mater.* **2002**, *14*, 147−151. (e) Wong, K. M.-C.; Zhu, X.; Hung, L.-L.; Zhu, N.; Yam, V. W.-W.; Kwok, H.-S. *Chem. Commun.* **2005**, 2906−2908. (f) Chen, Y.-L.; Li, S.-W.; Cheng, Y.-M.; Pu, S.-C.; Yeh, Y.-S.; Chou, P.-T. *ChemPhysChem* **2005**, *6*, 2012−2017.

(10) (a) D'Andrade, B. W.; Brooks, J.; Adamovich, V.; Thompson, M. E.; Forrest, S. R. *Adv. Mater.* **2002**, *14*, 1032−1036. (b) Adamovich, V.; Brooks, J.; Tamayo, A.; Alexander, A. M.; Djurovich, P. R.; D'Andrade, B. W.; Adachi, C.; Forrest, S. R.; Thompson, M. E. *New J. Chem.* **2002**, *26*, 1171−1178.

(11) (a) Lundin, N. J.; Blackman, A. G.; Gordon, K. C.; Officer, D. L. *Angew. Chem., Int. Ed.* **2006**, *45*, 2582−2584. (b) Chisholm, M. H.; Epstein, A. J.; Gallucci, J. C.; Feil, F.; Pirkle, W. *Angew. Chem., Int. Ed.* **2005**, *44*, 6537−6540. (c) Gong, X.; Ng, P. K.; Chan, W. K. *Adv. Mater.* **1998**, *10*, 1337−1340. (d) Wong, W.-Y.; He, Z.; So, S.-K.; Tong, K.-L.; Lin, Z. *Organometallics* **2005**, *24*, 4079−4082. (e) Liu, Z.; Guan, M.; Bian, Z.; Nie, D.; Gong, Z.; Li, Z.; Huang, C. *Adv. Funct. Mater.* **2006**, *16*, 1441−1448.

(12) (a) Kulkarni, A. P.; Tonzola, C. J.; Babel, A.; Jenekhe, S. A. *Chem. Mater.* **2004**, *16*, 4556−4573. (b) Furuta, P. T.; Deng, L.; Garon, S.; Thompson, M. E.; Fréchet, J. M. J. *J. Am. Chem. Soc.* **2004**, *126*, 15388−15389. (c) Suzuki, M.; Tokito, S.; Sato, F.; Igarashi, T.; Kondo, K.; Koyama, T.; Yamaguchi, T. *Appl. Phys. Lett.* **2005**, *86*, 103507-1−103507-3. (d) Ng, P. K.; Gong, X.; Chan, S. H.; Lam, L. S. M.; Chan, W. K. *Chem.−Eur. J.* **2001**, *7*, 4358−4367. (e) Manners, I. *Synthetic Metal-Containing Polymers*; Wiley-VCH: Weinheim, Germany, 2004.

realization of WOLEDs. We also report in this contribution the achievement of well-balanced white emission from an emissive layer with only a single luminescent dopant, which emits simultaneously from singlet and triplet excited states.

Experimental Section

General Comments. All reactions were carried out under a N_2 atmosphere with the use of standard Schlenk techniques, but no special precautions were taken to exclude O_2 during the workup. Solvents were predried and distilled from appropriate drying agents. All chemicals, unless otherwise stated, were obtained from commercial sources and used as received. Preparative thin layer chromatography (TLC) was performed on 0.7-mm silica plates (Merck Kieselgel 60 GF$_{254}$) prepared in our laboratory. ^{1}H and ^{13}C NMR spectra were measured in appropriate solvents on a JEOL EX270 or a Varian INOVA 400-MHz Fourier transform NMR spectrometer, with the chemical shifts quoted relative to SiMe$_4$. Fast atom bombardment mass spectrometry (FABMS) spectra were recorded on a Finnigan MAT SSQ710 mass spectrometer. Electronic absorption spectra were obtained with a Hewlett-Packard 8453 UV−visible spectrometer. For solid-state thin-film emission measurement, the 325-nm line of a He−Cd laser was used as an excitation source. The luminescence spectra were analyzed by a 0.25-m-focal-length double monochromator with a Peltier cooled photomultiplier tube and processed with a lock-in amplifier. The solution emission spectra and lifetimes were measured on a Photon Technology International Fluorescence Master Series QM1 spectrophotometer using an Xe lamp and a N_2 laser as the excitation source, respectively. The fluorescence quantum yields were determined in CH_2Cl_2 solutions at 298 K against the anthracene standard ($\Phi = 0.27$).[14] Thermal analyses were performed with the Perkin-Elmer TGA6 thermal analyzer at a heating rate of 20 °C min^{-1}. Theoretical calculations based on the density functional theory (DFT) approach at the B3LYP level were performed with the use of the *Gaussian03* program.[15] Experimental structures, whenever available, were used in the calculations. The geometry of **6-OMe** was derived from the X-ray structure of **7-OMe**, whereas that of **10** was derived from the X-ray structure of **11**. The basis set used for C, N, O, and H atoms was 6-31G, while effective core potentials with a LanL2DZ basis set were employed for the Pt atom.[16] Polarization functions were added for the P atom [$\zeta_d(P) = 0.34$]. All of the molecular orbital plots were made with the use of *Molden*, version 3.5.[17] The syntheses of **1-R**−**5-R** (R = F, H, Me, OMe) are shown in the Supporting Information.

6-F. A mixture of 2-(tri-*n*-butylstannyl)pyridine (0.53 g, 1.43 mmol), Pd(PPh$_3$)$_4$ (0.10 g, 0.09 mmol), and **5-F** (0.46 g, 0.92 mmol) was stirred in toluene (20 mL), and the mixture was heated to

110 °C for 50 h. Upon cooling to room temperature, the solvent was removed by rotary evaporation and the residue was purified by column chromatography using CH_2Cl_2 as the eluent to afford the title compound as a yellow powder (0.28 g, 61%). ^{1}H NMR (CDCl$_3$): δ 8.74−8.72 (m, 1H, Ar), 8.23−8.15 (m, 4H, Ar), 7.97−7.93 (m, 2H, Ar), 7.82−7.80 (m, 2H, Ar), 7.32−7.27 (m, 1H, Ar), 7.16−7.11 (m, 4H, Ar), 7.07−7.00 (m, 6H, Ar). ^{13}C NMR (CDCl$_3$): δ 164.58, 163.81, 160.93, 158.49, 155.97, 150.93, 149.88, 142.46, 142.43, 142.11, 136.94, 128.15, 127.46, 127.42, 127.38, 127.15, 124.27, 122.84, 120.77, 119.87, 116.70, 116.48, 115.80 (Ar). FABMS: *m/z* 503 (M$^+$). Anal. Calcd for C$_{31}$H$_{20}$N$_4$F$_2$O: C, 74.09; H, 4.01; N, 11.15. Found: C, 73,98; H, 4.08; N, 11.02.

6-H. Yield: yellow powder, 48% [CH$_2$Cl$_2$/ethyl acetate (5:1, v/v)]. ^{1}H NMR (CDCl$_3$): δ 8.75−8.72 (m, 1H, Ar), 8.24−8.15 (m, 4H, Ar), 7.99−7.94 (m, 2H, Ar), 7.82−7.79 (m, 2H, Ar), 7.36−7.27 (m, 5H, Ar), 7.19−7.09 (m, 8H, Ar). ^{13}C NMR (CDCl$_3$): δ 164.54, 163.64, 155.87, 150.85, 149.76, 146.49, 141.98, 136.82, 129.49, 127.95, 127.34, 127.07, 125.59, 124.31, 124.26, 122.73, 120.97, 120.69, 115.88 (Ar). FAB-MS: *m/z* 467 (M$^+$). Anal. Calcd for C$_{31}$H$_{22}$N$_4$O: C, 79.81; H, 4.75; N, 12.01. Found: C, 79.87; H, 4.56; N, 11.89.

6-Me. Yield: yellow solid, 85% [CH$_2$Cl$_2$/ethyl acetate (5:1, v/v)]. ^{1}H NMR (CDCl$_3$): δ 8.70−8.69 (m, 1H, Ar), 8.20−8.11 (m, 4H, Ar), 7.91−7.88 (m, 2H, Ar), 7.76−7.73 (m, 2H, Ar), 7.26−7.21 (m, 1H, Ar), 7.13−7.01 (m, 10H, Ar), 2.33 (s, 6H, CH$_3$). ^{13}C NMR (CDCl$_3$): δ 164.48, 163.32, 155.62, 150.98, 149.56, 143.72, 141.70, 136.65, 133.98, 129.99, 127.72, 127.14, 126.84, 125.62, 124.14, 122.57, 120.48, 119.50, 114.72 (Ar), 20.89 (CH$_3$). FABMS: *m/z* 495 (M$^+$). Anal. Calcd for C$_{33}$H$_{26}$N$_4$O: C, 80.14; H, 5.30; N, 11.33. Found: C, 80.20; H, 5.15; N, 11.16.

6-OMe. Yield: yellow solid, 67% [CH$_2$Cl$_2$/ethyl acetate (10:1, v/v)]. ^{1}H NMR (CDCl$_3$): δ 8.74−8.72 (m, 1H, Ar), 8.23−8.14 (m, 4H, Ar), 7.91−7.88 (m, 2H, Ar), 7.81−7.79 (m, 2H, Ar), 7.31−7.26 (m, 1H, Ar), 7.15−7.12 (m, 4H, Ar), 6.96−6.87 (m, 6H, Ar), 3.82 (s, 6H, OCH$_3$). ^{13}C NMR (CDCl$_3$): δ 164.76, 163.42, 156.71, 155.92, 151.58, 149.74, 141.87, 139.32, 136.79, 127.90, 127.53, 127.30, 127.01, 124.38, 122.69, 120.66, 118.06, 114.89, 114.05 (Ar), 55.52 (OCH$_3$). FABMS: *m/z* 527 (M$^+$). Anal. Calcd for C$_{33}$H$_{26}$N$_4$O$_3$: C, 75.27; H, 4.98; N, 10.64. Found: C, 75.11; H, 5.08; N, 10.44.

7-F. A mixture of **6-F** (0.10 g, 0.20 mmol) and K$_2$PtCl$_4$ (0.04 g, 0.10 mmol) was stirred in 2-ethoxyethanol (6 mL) and water (2 mL), and the suspension was heated to 80 °C for 16 h. After cooling to room temperature, it was added to water (20 mL), and the precipitate collected was washed with water (20 mL × 4) and

(13) (a) Tokito, S.; Iijima, T.; Tsuzuki, T.; Sato, F. *Appl. Phys. Lett.* **2003**, *83*, 2459−2461. (b) Gong, X.; Wang, S.; Moses, D.; Bazan, G. C.; Heeger, A. J. *Adv. Mater.* **2005**, *17*, 2053−2058. (c) Tu, G.; Mei, C.; Zhou, Q.; Cheng, Y.; Geng, Y.; Wang, L.; Ma, D.; Jing, X.; Wang, F. *Adv. Funct. Mater.* **2006**, *16*, 101−106. (d) Liu, J.; Zhou, Q.; Cheng, Y.; Geng, Y.; Wang, L.; Ma, D.; Jing, X.; Wang, F. *Adv. Funct. Mater.* **2006**, *16*, 957−965. (e) D'Andrade, B. W.; Holmes, R. J.; Forrest, S. R. *Adv. Mater.* **2004**, *16*, 624−628. (f) Chuen, C. H.; Tao, Y. T. *Appl. Phys. Lett.* **2002**, *81*, 4499−4501. (g) Gong, X.; Ma, W.; Ostrowski, J. C.; Bazan, G. C.; Moses, D.; Heeger, A. J. *Adv. Mater.* **2004**, *16*, 615−619. (h) Lei, G.; Wang, L.; Qiu, Y. *Appl. Phys. Lett.* **2004**, *85*, 5403−5405. (i) Sun, Y.; Giebink, N. C.; Kanno, H.; Ma, B.; Thompson, M. E.; Forrest, S. R. *Nature* **2006**, *440*, 908−912. (j) Heeger, A. J. *Solid State Commun.* **1998**, *107*, 673−679. (k) Shih, P.-I.; Shu, C.-F.; Tung, Y.-L.; Chi, Y. *Appl. Phys. Lett.* **2006**, *88*, 251110-1−251110-3.

(14) Dawson, W. R.; Windsor, M. W. *J. Phys. Chem.* **1968**, *72*, 3251−3260.

(15) Frisch, M. J.; Trucks, G. W.; Schlegel, H. B.; Scuseria, G. E.; Robb, M. A.; Cheeseman, J. R.; Montgomery, J. A.; Vreven, T.; Kudin, K. N.; Burant, J. C.; Millam, J. M.; Iyengar, S. S.; Tomasi, J.; Barone, V.; Mennucci, B.; Cossi, M.; Scalmani, G.; Rega, N.; Petersson, G. A.; Nakatsuji, H.; Hada, M.; Ehara, M.; Toyota, K.; Fukuda, R.; Hasegawa, J.; Ishida, M.; Nakajima, T.; Honda, Y.; Kitao, O.; Nakai, H.; Klene, M.; Li, X.; Knox, J. E.; Hratchian, H. P.; Cross, J. B.; Adamo, C.; Jaramillo, J.; Gomperts, R.; Stratmann, R. E.; Yazyev, O.; Austin, A. J.; Cammi, R.; Pomelli, C.; Ochterski, J. W.; Ayala, P.; Morokuma, Y. K.; Voth, G. A.; Salvador, P.; Dannenberg, J. J.; Zakrzewski, V. G.; Dapprich, S.; Daniels, A. D.; Strain, M. C.; Farkas, O.; Malick, D. K.; Rabuck, A. D.; Raghavachari, K.; Foresman, J. B.; Ortiz, J. V.; Cui, Q.; Baboul, A. G.; Clifford, S.; Cioslowski, J.; Stefanov, B. B.; Liu, G.; Liashenko, A.; Piskorz, P.; Komaromi, I.; Martin, R. L.; Fox, D. J.; Keith, T.; Al-Laham, M. A.; Peng, C. Y.; Nanayakkara, A.; Challacombe, M.; Gill, P. M. W.; Johnson, B.; Chen, W.; Wong, M. W.; Gonzalez, C.; Pople, J. A. *Gaussian03*, revision B05; Gaussian, Inc.: Pittsburgh, PA, 2003.

(16) (a) Wadt, W. R.; Hay, P. J. *J. Chem. Phys.* **1985**, *82*, 284−298. (b) Hay, P. J.; Wadt, W. R. *J. Chem. Phys.* **1985**, *82*, 299−310.

(17) Schaftenaar, G. *Molden*, version 3.5; CAOS/CAMM Center Nijmegen, Toernooiveld: Nijmegen, The Netherlands, 1999.

vacuum dried. The precipitate then reacted with acetylacetone (Hacac; 0.03 mL, 0.30 mmol) and Na_2CO_3 (0.11 g, 1.00 mmol) in 2-ethoxyethanol (8 mL) at 100 °C for 16 h. The solvent was removed under reduced pressure, and the residue was purified by preparative TLC plates on silica using CH_2Cl_2/ethyl acetate (10:1, v/v) as the eluent to afford a yellow product with an isolated yield of 50% (0.04 g, 0.05 mmol). ^{1}H NMR (CDCl$_3$): δ 9.02–9.00 (d, 1H, Ar), 8.25–8.25 (d, 1H, Ar), 7.95–7.92 (m, 2H, Ar), 7.88–7.81 (m, 2H, Ar), 7.66–7.64 (d, 1H, Ar), 7.53–7.50 (d, 1H, Ar), 7.18–7.11 (m, 5H, Ar), 7.07–7.00 (m, 6H, Ar), 5.49 (s, 1H, CH), 2.06 (s, 3H, CH$_3$), 2.01 (s, 3H, CH$_3$). ^{13}C NMR (CDCl$_3$): δ 185.84, 184.26, 166.92, 164.48, 164.35, 160.87, 158.43, 150.74, 147.81, 147.48, 142.57, 142.55, 139.39, 138.30, 128.15, 128.04, 127.41, 127.33, 123.52, 123.09, 122.33, 122.06, 120.03, 119.10, 116.68, 116.46, 116.25 (Ar), 102.61 (CH), 28.21, 27.24 (CH$_3$). FABMS: m/z 796 (M$^+$). Anal. Calcd for C$_{36}$H$_{26}$N$_4$F$_2$O$_3$Pt: C, 54.34; H, 3.29; N, 7.04. Found: C, 54.10; H, 3.53; N, 6.87.

7-H. Yield: yellow solid, 58% (eluent: CH_2Cl_2). ^{1}H NMR (CDCl$_3$): δ 9.03–9.01 (d, 1H, Ar), 8.27–8.26 (d, 1H, Ar), 7.97–7.80 (m, 4H, Ar), 7.67–7.64 (d, 1H, Ar), 7.54–7.51 (d, 1H, Ar), 7.36–7.26 (m, 4H, Ar), 7.19–7.10 (m, 9H, Ar), 5.50 (s, 1H, CH), 2.06–2.02 (d, 6H, CH$_3$). ^{13}C NMR (CDCl$_3$): δ 185.64, 184.12, 166.81, 164.30, 150.65, 147.64, 147.37, 146.60, 139.28, 138.19, 129.48, 128.09, 127.85, 126.33, 125.54, 124.18, 123.51, 123.01, 122.27, 121.96, 121.16, 119.01, 116.36 (Ar), 102.56 (CH), 28.29, 27.35 (CH$_3$). FABMS: m/z 760 (M$^+$). Anal. Calcd for C$_{36}$H$_{28}$N$_4$O$_3$Pt: C, 56.91; H, 3.71; N, 7.37. Found: C, 56.76; H, 3.55; N, 7.16.

7-Me. Yield: yellow solid, 36% (eluent: CH_2Cl_2). ^{1}H NMR (CDCl$_3$): δ 9.02–9.00 (d, 1H, Ar), 8.25–8.24 (d, 1H, Ar), 7.92–7.80 (m, 4H, Ar), 7.66–7.63 (d, 1H, Ar), 7.53–7.50 (d, 1H, Ar), 7.15–7.03 (m, 11H, Ar), 5.49 (s, 1H, CH), 2.35 (s, 6H, CH$_3$), 2.06–2.01 (d, 6H, CH$_3$). ^{13}C NMR (CDCl$_3$): δ 185.62, 184.12, 166.84, 164.44, 164.19, 150.97, 147.58, 147.35, 144.01, 139.27, 138.16, 134.01, 130.09, 128.05, 127.76, 125.72, 123.57, 122.99, 122.24, 121.92, 119.90, 118.99, 115.37 (Ar), 102.53 (CH), 28.28, 27.34, 21.00 (CH$_3$). FABMS: m/z 788 (M$^+$). Anal. Calcd for C$_{38}$H$_{32}$N$_4$O$_3$Pt: C, 57.94; H, 4.09; N, 7.11. Found: C, 57.68; H, 3.96; N, 7.05.

7-OMe. Yield: yellow solid, 44% (eluent: CH_2Cl_2). ^{1}H NMR (CDCl$_3$): δ 9.05–9.03 (d, 1H, Ar), 8.27–8.26 (d, 1H, Ar), 7.91–7.83 (m, 4H, Ar), 7.69–7.66 (d, 1H, Ar), 7.56–7.53 (d, 1H, Ar), 7.21–7.10 (m, 5H, Ar), 6.96–6.87 (m, 6H, Ar), 5.51 (s, 1H, CH), 3.82 (s, 6H, OCH$_3$), 2.07–2.03 (d, 6H, CH$_3$). ^{13}C NMR (CDCl$_3$): δ 185.67, 184.19, 166.90, 164.54, 164.10, 156.62, 151.40, 147.53, 147.40, 139.45, 139.19, 138.22, 128.07, 127.81, 127.52, 123.69, 123.02, 122.29, 121.94, 119.00, 118.20, 114.86, 114.50 (Ar), 102.56 (CH), 55.53 (OCH$_3$), 28.29, 27.36 (CH$_3$). FABMS: m/z 820 (M$^+$). Anal. Calcd for C$_{38}$H$_{32}$N$_4$O$_5$Pt: C, 55.68; H, 3.93; N, 6.83. Found: C, 55.50; H, 3.68; N, 6.55.

8. A mixture of 2-(tri-*n*-butylstannyl)pyridine (0.75 g, 2.04 mmol), Pd(PPh$_3$)$_4$ (0.05 g, 0.08 mmol), and (4-iodophenyl)diphenylamine[18] (0.50 g, 1.35 mmol) was combined in toluene (30 mL), and the mixture was heated to 110 °C for 48 h. Upon cooling to room temperature and removal of the solvent, the residue was purified by column chromatography using CH_2Cl_2 as the eluent to afford a yellow solid of **8** in 58% yield (0.25 g). ^{1}H NMR (CDCl$_3$): δ 8.65–8.63 (m, 1H, Ar), 7.87–7.84 (m, 2H, Ar), 7.73–7.65 (m, 2H, Ar), 7.29–7.21 (m, 4H, Ar), 7.18–7.16 (m, 7H, Ar), 7.09–7.02 (m, 2H, Ar). ^{13}C NMR (CDCl$_3$): δ 157.02, 149.55, 148.62, 147.42, 136.62, 133.07, 129.27, 127.68, 124.67, 123.17, 121.43, 119.84

(18) Kato, S.-I.; Matsumoto, T.; Ishi-I, T.; Thiemann, T.; Shigeiwa, M.; Gorohmaru, H.; Maeda, S.; Yamashita, Y.; Mataka, S. *Chem. Commun.* **2004**, 2342–2343.

(Ar). FABMS: m/z 322 (M$^+$). Anal. Calcd for C$_{23}$H$_{18}$N$_2$: C, 85.68; H, 5.63; N, 8.69. Found: C, 85.70; H, 5.48; N, 8.55.

9. A mixture of **8** (0.20 g, 0.63 mmol) and K$_2$PtCl$_4$ (0.10 g, 0.25 mmol) in 2-ethoxyethanol (6 mL) and water (2 mL) was heated to 80 °C for 16 h. After cooling to room temperature, it was added to water (20 mL) and the precipitate was washed with water (20 mL × 4) and dried under vacuum. Reaction of the precipitate with Hacac (0.036 g, 0.36 mmol), in the presence of Na$_2$CO$_3$ (0.13 g, 1.20 mmol), in 2-ethoxyethanol (6 mL) at 100 °C for 20 h gave a residue that was purified by preparative TLC plates on silica, eluting with CH_2Cl_2 to afford the product as a yellow solid in 24% yield (0.037 g). ^{1}H NMR (CDCl$_3$): δ 8.88–8.87 (m, 1H, Ar), 7.73–7.69 (m, 1H, Ar), 7.47–7.45 (d, 1H, Ar), 7.29–7.24 (m, 6H, Ar), 7.22–7.17 (m, 4H, Ar), 7.06–6.97 (m, 3H, Ar), 6.78–6.75 (m, 1H, Ar), 5.30 (s, 1H, CH), 1.96 (s, 3H, CH$_3$), 1.72 (s, 3H, CH$_3$). ^{13}C NMR (CDCl$_3$): δ 185.61, 184.01, 167.76, 148.34, 147.45, 147.09, 139.80, 137.94, 137.84, 129.08, 125.41, 123.90, 123.13, 122.95, 119.79, 117.64, 117.48 (Ar), 102.29 (CH), 28.24, 26.82 (CH$_3$). FABMS: m/z 616 (M$^+$). Anal. Calcd for C$_{28}$H$_{24}$N$_2$O$_2$Pt: C, 54.63; H, 3.93; N, 4.55. Found: C, 54.34; H, 3.61; N, 4.27.

10. A mixture of 2-(tri-*n*-butylstannyl)pyridine (0.75 g, 2.50 mmol), Pd(PPh$_3$)$_4$ (0.09 g, 0.08 mmol), and (2-phenyl)-5-[1-(2-bromo)-4-phenyl]-1,3,4-oxadiazole[19] (0.92 g, 2.50 mmol) in toluene (20 mL) was heated to 110 °C for 48 h. Upon cooling to room temperature, the solvent was removed by rotary evaporation and the residue was purified by column chromatography using CH_2-Cl$_2$/hexane (6:1, v/v) as the eluent to afford a yellow powder of **10** (0.66 g, 88%). ^{1}H NMR (CDCl$_3$): δ 8.75–8.73 (d, 1H, Ar), 8.27–8.15 (m, 6H, Ar), 7.82–7.80 (d, 2H, Ar), 7.56–7.52 (m, 3H, Ar), 7.32–7.26 (m, 1H, Ar). ^{13}C NMR (CDCl$_3$): δ 164.48, 164.20, 155.76, 149.75, 142.20, 136.82, 131.64, 128.96, 127.35, 127.19, 126.84, 124.00, 123.75, 122.79, 120.71 (Ar). FABMS: m/z 300 (M$^+$). Anal. Calcd for C$_{19}$H$_{13}$N$_3$O: C, 76.24; H, 4.38; N, 14.04. Found: C, 76.10; H, 4.12; N, 13.86.

11: A mixture of **10** (0.09 g, 0.24 mmol) and K$_2$PtCl$_4$ (0.05 mg, 0.12 mmol) in 2-ethoxyethanol (6 mL) and water (2 mL) was allowed to react at 80 °C for 16 h. After cooling to room temperature, it was added to water (20 mL), and the precipitate obtained was washed with water (20 mL × 4) and dried over anhydrous MgSO$_4$. Then, the precipitate reacted with Hacac (0.03 g, 0.30 mmol) and Na$_2$CO$_3$ (0.106 g, 1.00 mmol) in 2-ethoxyethanol (8 mL) at 100 °C for 20 h. The solvent was removed under reduced pressure, and purification of the residue was achieved by preparative TLC plates on silica using CH_2Cl_2 as the eluent to afford the desired product as a yellow solid in 90% yield (0.06 g). ^{1}H NMR (CDCl$_3$): δ 9.06–9.04 (d, 1H, Ar), 8.34–8.33 (d, 1H, Ar), 8.17–8.14 (m, 2H, Ar), 7.94–7.84 (m, 2H, Ar), 7.71–7.68 (d, 1H, Ar), 7.58–7.53 (m, 4H, Ar), 7.22–7.18 (m, 1H, Ar), 5.53 (s, 1H, CH), 2.11 (s, 3H, CH$_3$), 2.04 (s, 3H, CH$_3$). ^{13}C NMR (CDCl$_3$): δ 185.74, 184.23, 166.85, 164.90, 164.31, 147.45, 139.32, 138.26, 131.43, 128.94, 128.37, 127.41, 126.81, 124.14, 123.38, 123.03, 122.44, 122.07, 119.08 (Ar), 102.60 (CH), 28.30, 27.31 (CH$_3$). FABMS: m/z 593 (M$^+$). Anal. Calcd for C$_{24}$H$_{19}$N$_3$O$_3$Pt: C, 48.65; H, 3.23; N, 7.09. Found: C, 48.43; H, 3.01; N, 6.78.

Electrochemical Measurements. Electrochemical measurements were made using a BAS CV-50W model potentiostat. A conventional three-electrode configuration consisting of a Pt working electrode, a Pt-wire counter electrode, and an Ag/AgCl reference electrode was used. The solvent in all measurements was CH_2Cl_2, and the supporting electrolyte was 0.1 M [Bu$_4$N]PF$_6$. Ferrocene was added as a calibrant after each set of measurements, and all

(19) Hou, S.; Chan, W. K. *Macromolecules* **2002**, *35*, 850–856.

Table 1. Summary of the Crystal Structure Data

	6-F	7-F·CH₂Cl₂	7-H·H₂O	7-Me·CH₂Cl₂	7-OMe·CH₂Cl₂	9	11
formula	$C_{31}H_{20}N_4F_2O$	$C_{37}H_{28}N_4Cl_2$-F_2O_3Pt	$C_{36}H_{30}N_4O_4Pt$	$C_{39}H_{34}N_4Cl_2$-O_3Pt	$C_{39}H_{34}N_4Cl_2$-O_5Pt	$C_{28}H_{24}N_2O_2Pt$	$C_{24}H_{19}N_3O_3Pt$
M_r	502.51	880.62	777.73	872.69	904.69	615.58	592.51
cryst size [mm]	0.30 × 0.25 × 0.23	0.30 × 0.26 × 0.12	0.30 × 0.26 × 0.12	0.34 × 0.26 × 0.24	0.30 × 0.25 × 0.20	0.24 × 0.20 × 0.14	0.28 × 0.20 × 0.10
cryst syst	triclinic	triclinic	monoclinic	triclinic	triclinic	monoclinic	orthorhombic
space group	$P\bar{1}$	$P\bar{1}$	$P2_1/c$	$P\bar{1}$	$P\bar{1}$	$P2_1/c$	$Pca2_1$
a (Å)	9.3204(7)	12.5305(7)	19.827(9)	9.9455(6)	10.8475(4)	13.4384(7)	24.5142(17)
b (Å)	11.9915(9)	16.5828(9)	13.692(6)	13.5126(8)	18.5133(7)	9.5829(5)	4.9526(3)
c (Å)	12.1553(9)	18.2259(10)	11.835(6)	14.3504(8)	19.3000(8)	18.3541(10)	34.174(2)
α (deg)	73.676(1)	68.0830(10)	90	105.2070(10)	102.6460(10)	90	90
β (deg)	83.694(1)	87.4360(10)	97.041(10)	103.1460(10)	100.2840(10)	103.2660(10)	90
γ (deg)	77.613(1)	81.3220(10)	90	90.1550(10)	93.1570(10)	90	90
V (Å³)	1271.7(2)	3473.0(3)	3189(3)	1808.3(2)	3703.2(2)	2300.5(2)	4149.0(5)
Z	2	4	4	2	4	4	8
D_{calcd} (g cm⁻³)	1.312	1.684	1.620	1.603	1.623	1.777	1.897
μ (mm⁻¹)	0.092	4.247	4.446	4.070	3.982	6.127	6.796
$F(000)$	520	1728	1536	864	1792	1200	2288
θ range (deg)	1.80−28.25	1.43−25.00	1.81−25.00	1.86−25.00	1.38−25.00	2.28−28.29	1.66−25.00
no. of reflns collected	7611	17447	15455	9030	18499	13298	19085
no. of unique reflns	5523	12046	5589	6239	12783	5345	7064
R_{int}	0.0142	0.0414	0.1077	0.0154	0.0179	0.0361	0.0625
no. of reflns with $I > 2.0\sigma(I)$	3078	7292	2932	5708	10327	3853	5064
no. of params	343	883	407	442	914	298	559
R1 [$I > 2.0\sigma(I)$][a]	0.0480	0.0469	0.0603	0.0227	0.0340	0.0304	0.0453
wR2 (all data)[a]	0.1586	0.1131	0.1651	0.0590	0.0969	0.0647	0.1105
GOF on F^2[b]	0.996	0.953	0.925	1.031	1.012	1.039	0.990

[a] $R1 = \sum||F_o| - |F_c||/\sum|F_o|$. $wR2 = \{\sum[w(F_o^2 - F_c^2)^2]/\sum[w(F_o^2)^2]\}^{1/2}$. [b] $GOF = [(\sum w|F_o| - |F_c|)^2/(N_{obs} - N_{param})]^{1/2}$.

potentials reported were quoted with reference to the ferrocene/ferrocenium (Fc/Fc⁺) couple at a scan rate of 100 mV s⁻¹.

Crystallography. Single crystals suitable for X-ray crystallographic analyses were grown by slow evaporation of their respective solutions in CH_2Cl_2/n-hexane at room temperature. Important crystal data pertinent to individual compounds and the structure refinement results are assemblied in Table 1. The diffraction experiments were carried out at 293 K on a Bruker Axs SMART 1000 CCD area detector diffractometer using graphite-monochromated Mo Kα radiation (λ = 0.710 73 Å). The raw intensity data frames were integrated with the SAINT+ program using a narrow-frame integration algorithm.[20] Corrections for Lorentz and polarization effects were also applied by SAINT. For each analysis, an empirical absorption correction based on the multiple measurement of equivalent reflections was applied by using the program SADABS.[21] The structures were solved by direct methods and expanded by difference Fourier syntheses using the software SHELXTL.[22] Structure refinements were made on F^2 by the full-matrix least-squares technique. All non-H atoms were refined with anisotropic displacement parameters. The H atoms were placed in their ideal positions but not refined.

Results and Discussion

Synthesis and Characterization. Scheme 1 shows the chemical structure and synthetic strategies to the integrated Pt(II) complexes containing all three functionalities in the present study. First, the N-arylation of aniline was carried out by the modified Ullmann condensation with the corresponding p-iodoarene under the CuCl/phen/KOH catalytic system to give the substituted triarylamines **1-R**.[23] Formylation of **1-R** with POCl₃ in N,N-dimethylformamide affords **2-R**, which can be derivatized to **3-R** using a hydroxylamine hydrochloride/acetic acid/pyridine mixture and then to **4-R** via the use of NaN₃/NH₄Cl. The key bipolar ligands **6-R** in this work can be obtained from 4-tetrazoyltriphenylamine **4-R**[6a] by a two-step reaction. Compounds **4-R** react with 4-bromobenzoyl chloride to give **5-R**, which can then undergo Stille coupling with 2-(tri-n-butylstannyl)pyridine to afford **6-R**, carrying a cyclometalating 2-phenylpyridine site for coordination with the Pt(II) ion. Reaction of K₂PtCl₄ with **6** in a mixture of 2-ethoxyethanol and water results in the dinuclear chloro-bridged Pt(II) complex, which is cleaved with Hacac in the presence of a base to give the corresponding mononuclear complex **7-R**.[24] The design rationale of the trifunctional molecule **7-R** lies in the notion that [Pt(ppy)-(acac)]-type complexes (ppy = 2-phenylpyridyl anion) are known to be highly emissive and have been used as triplet-emitting dopants in a variety of OLED structures.[10,12b,24b] 1,3,4-Oxadiazole heterocycles are widely used as ET groups owing to their electron deficiency and good thermal stability.[2c,25] The triarylamine subunit can act as a HT group and can also be easily functionalized by chemical means.[26]

(20) SAINT+, version 6.02a; Bruker Analytical X-ray System, Inc.: Madison, WI, 1998.

(21) Sheldrick, G. M. SADABS, Empirical Absorption Correction Program; University of Göttingen: Göttingen, Germany, 1997.

(22) Sheldrick, G. M. SHELXTL^TM, Reference Manual, version 5.1; Madison, WI, 1997.

(23) (a) Hassan, J.; Sévignon, M.; Gozzi, C.; Schulz, E.; Lemaire, M. Chem. Rev. **2002**, 102, 1359−1470. (b) Martínez-Palau, M.; Perea, E.; López-Calahorra, F.; Velasco, D. Lett. Org. Chem. **2004**, 1, 231−237.

(24) (a) Brooks, J.; Babayan, Y.; Lamansky, S.; Djurovich, P. I.; Tsyba, I.; Bau, R.; Thompson, M. E. Inorg. Chem. **2002**, 41, 3055−3066. (b) Laskar, I. R.; Hsu, S.-F.; Chen, T.-M. Polyhedron **2005**, 24, 881−888.

Scheme 1. Synthesis of Multifunctional Pt(II) Complexes and Their Ligand Precursors
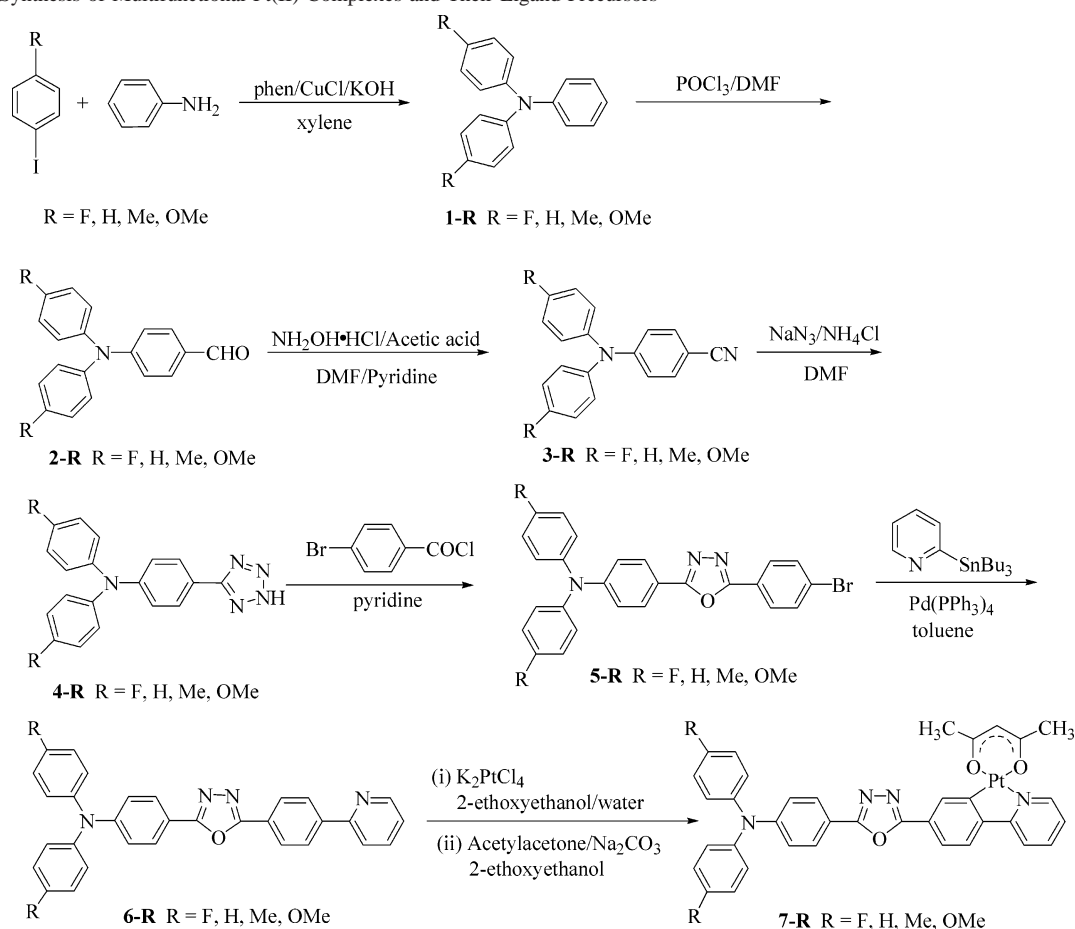
These modular units were covalently linked to form trifunctional molecules as outlined in Scheme 1. For comparison, complexes **9** and **11** were also prepared as model compounds to examine the effects of each of the individual oxadiazole and aromatic amine moieties. They differ from **7-H** in that complex **9** does not contain an oxadiazole ring whereas the arylamine unit is absent in **11**. Coupling of the 2-pyridyl unit with a suitable halo-substituted triphenylamine or 2,5-diphenyloxadiazole chromophore can furnish **8** and **10**, which can be employed to give **9** and **10** following the classical cyclometalation synthetic protocol (Scheme 2).[24] The crude products from these reaction mixtures were purified by column chromatography or preparative TLC on silica and recrystallized where necessary.

All of the new metal complexes are air-stable orange crystalline solids and can be stored without any special precautions. They are found to be soluble in chlorinated solvents such as CH_2Cl_2 but are generally insoluble in hydrocarbons. They all gave satisfactory analytical data and were characterized by FABMS and NMR spectroscopy. The spectroscopic data shown in the Experimental Section are in line with their assigned structures.

Crystallography. The three-dimensional molecular structures of **6-F**, **7-F**, **7-H**, **7-Me**, **7-OMe**, **9**, and **11** were confirmed by X-ray crystallography, and Figure 1 illustrates perspective views of all of the Pt complexes. Pertinent bond distances and angles are given in Table 2. The crystal structures of these cycloplatinates reveal a typical four-coordinate Pt core with a square-planar geometry, and there is very little distortion away from the square plane for Pt. The oxadiazole ring and the Pt square plane differ from coplanarity by 6.0–18.6°. Intermolecular interactions in the crystal lattices of Pt(II) complexes are known to play a crucial role in their solid-state emission properties.[10] Except for **7-Me** and **11**, the lattice is characterized by the presence of Pt⋯Pt intermolecular interactions (ca. 3.240–3.741 Å) between adjacent molecules, and crystal packing effects may, among other not yet realized factors, contribute to this structural difference. This metal–metal interaction can be compared to those observed for other monocyclometalated π–π-stacked Pt(II) complexes containing a simpler 2-phenylpyridine moiety in the literature,[24,27] where the shortest Pt⋯Pt length reported is 3.528 Å.[27b] As noted below, these interactions may be invoked to rationalize the lower-energy

(25) Kulkarni, A. P.; Tonzola, C. J.; Babel, A.; Jenekhe, S. A. *Chem. Mater.* **2004**, *16*, 4556–4573.

(26) (a) Strohriegl, P.; Grazulevicius, J. V. *Adv. Mater.* **2002**, *14*, 1439–1452. (b) Hreha, R. D.; George, C. P.; Haldi, A.; Domercq, B.; Malagoli, M.; Barlow, S.; Brédas, J.-L.; Kippelen, B.; Marder, S. R. *Adv. Funct. Mater.* **2003**, *13*, 967–973. (c) Kunda, P.; Thomas, K. R. J.; Lin, J. T.; Tao, Y.-T.; Chien, C.-H. *Adv. Funct. Mater.* **2003**, *13*, 445–447.

(27) (a) Ma, B.; Li, J.; Djurovich, P. I.; Yousufuddin, M.; Bau, R.; Thompson, M. E. *J. Am. Chem. Soc.* **2005**, *127*, 28–29. (b) Chassot, L.; Muller, E.; von Zelewsky, A. *Inorg. Chem.* **1984**, *23*, 4249–4253.

Scheme 2. Synthesis of Some Model Pt(II) Complexes **9** and **10**
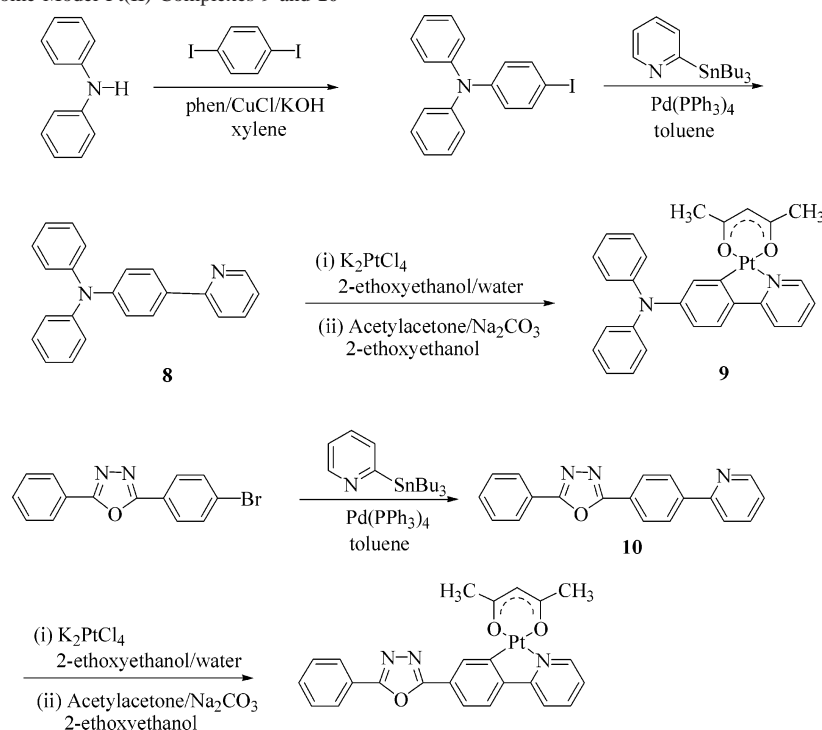
solid-state emissions displayed by complexes **7-R**, where appropriate. The bond length of Pt—N [1.955(11)−1.996(3) Å] is slightly longer compared to that of common Pt—N bonds because this N is opposite to the acac O atom having a weak trans influence. The bond distance of the Pt—O edge trans to C [2.064(11)−2.094(3) Å] is larger compared to that of the other Pt—O bond [1.991(9)−2.003(3) Å] because the O atom trans to C has a strong trans influence. All other bond lengths around the Pt core are typical for cyclometalates and β-diketonate derivatives of Pt(II).[24,27]

Thermal and Photophysical Properties. The thermal properties of the compounds were examined by thermogravimetric analysis (TGA). All of the pyridyl derivatives and their Pt(II) complexes generally exhibit high thermal stability, and their onset decomposition temperatures (T_{decomp}) range from 341 to 466 °C for the cyclometalating ligands and from 255 to 370 °C for the Pt complexes (Table 3). In addition, both series of **6-R** and **7-R** can be easily sublimed at low pressures (∼10⁻⁶ Pa) without decomposition. Hence, complexes **7-R** are sufficiently stable to be incorporated into multilayer OLEDs by the vacuum deposition method. However, complex **11** tends to degrade readily upon sublimation at reduced pressures and does not readily form a good solid thin film.

The absorption and emission data of the new metallized compounds **7-R** and their ligand precursors **6-R** are shown in Table 3. For **6-R**, two distinct absorption bands are observed at 293−296 and 364−375 nm, which may be attributed to the π−π* transitions associated with the N−Ar and N−C₆H₄−X fragments (Figure 2a). Similar data were observed by Low et al. in the spectra of Ar₂N−C₆H₄−X species near 300 and 350 nm.[28] An analogous ligand system containing a 2,2′-bipyridyl unit also shows absorption

features at 316 and 388 nm.[11c] However, we cannot rule out completely the possibility of a minor component for ligand-to-ligand charge transfer in these bands. For **7-R**, the lower energy absorption bands around 370−385 nm are notably red-shifted from the free ligand absorption because of perturbation from the metal but are not solvatochromic. Metal-centered d−d transitions are not observed for **7-R**, and it is likely that the strong ligand field of the cyclometalating ligands shifts the d−d transitions to high energy, putting them under the more intense ligand-centered (LC) transitions. While the higher energy absorption peak does not change with the R groups, the lower-lying band is slightly blue-shifted by electron-withdrawing units (λ_{max} = 364 nm) and red-shifted by electron-donating moieties (λ_{max} = 375 nm). Attachment of the Pt core into the ligand was shown to enrich the photoluminescent (PL) properties. The absorption spectra of **7-R** in CH₂Cl₂ also feature two intense bands at 293−295 and 370−385 nm in each case due to the LC transitions from the π orbitals of arylamine to the π* orbitals of oxadiazole-based 2-arylpyridine (Figure 2b). The ligand substituent effect is also operative for the lowest energy emission bands for **7-R**, in line with the absorption studies. These assignments were also supported by theoretical calculations for **6-R** and **7-R**, which reveal that the HOMO is basically triphenylamine-based and the LUMO predominantly corresponds to the π* orbitals of the 2-(2-arylpyridine)-1,3,4-oxadiazole group. The HOMO−1 level also contains substantial contribution from the Pt's d orbital

(28) (a) Low, P. J.; Paterson, M. A. J.; Goeta, A. E.; Yufit, D. S.; Howard, J. A. K.; Cherryman, J. C.; Tackley, D. R.; Brown, B. *J. Mater. Chem.* **2004**, *14*, 2516−2523. (b) Low, P. J. M.; Paterson, A. J.; Puschmann, H.; Goeta, A. E.; Howard, J. A. K.; Lambert, C.; Cherryman, J. C.; Tackley, D. R.; Leeming, S.; Brown, B. *Chem.—Eur. J.* **2004**, *10*, 83−91.
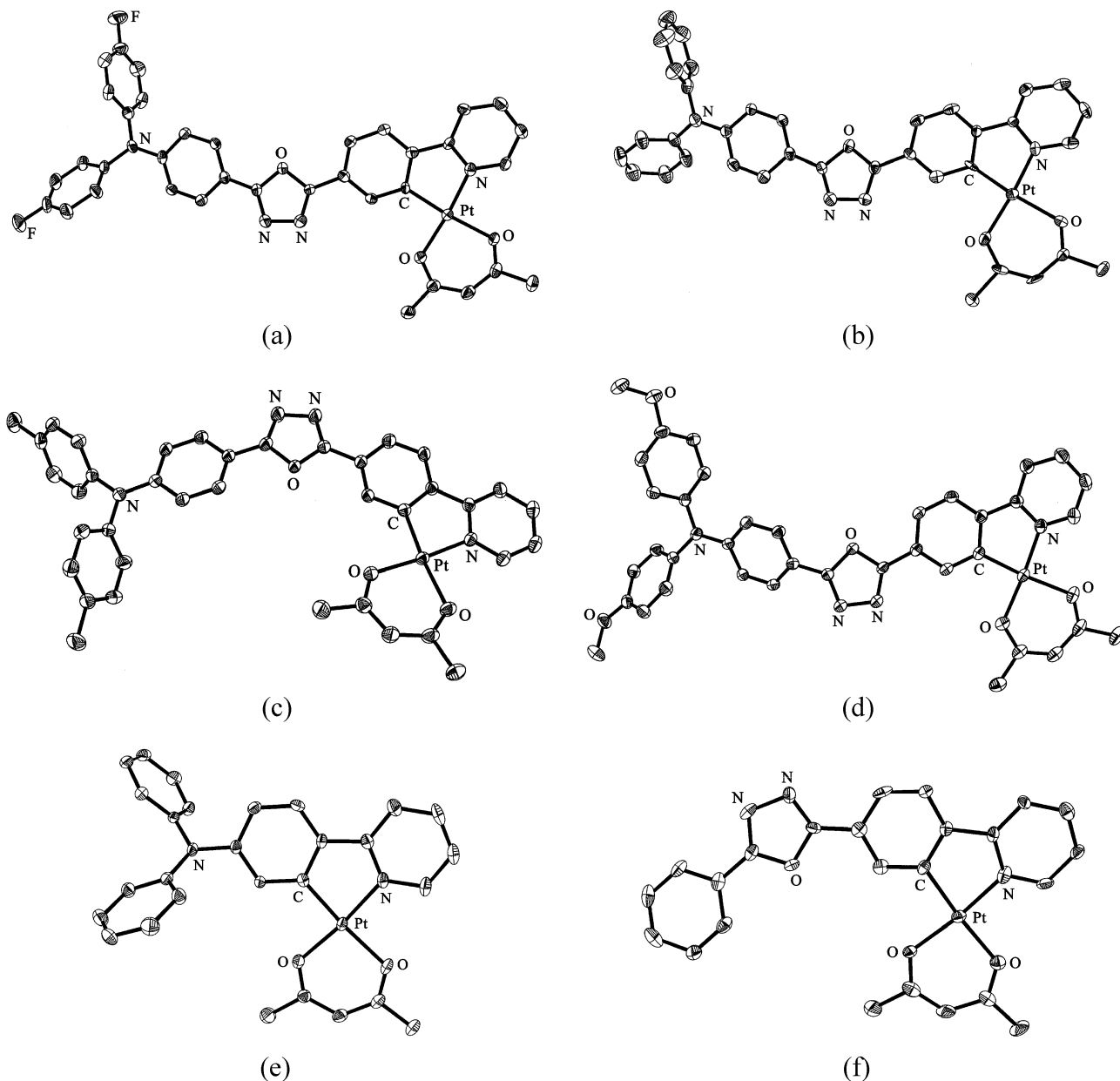
Figure 1. Perspective drawings of (a) **7-F**, (b) **7-H**, (c) **7-Me**, (d) **7-OMe**, (e) **9**, and (f) **11**. In each case, thermal ellipsoids are drawn at the 25% probability level. H atoms and all labels for the C atoms are omitted for clarity.

Table 2. Selected Bond Lengths (Å) and Angles (deg) around the Metal Core in **7-F**, **7-H**, **7-Me**, **7-OMe**, **9**, and **11**

	Pt−N	Pt−C	Pt−O	C−Pt−N	O−Pt−O	Pt···Pt
7-F	1.991(7)	1.980(8)	2.002(6) 2.077(6)	81.3(3)	92.0(2)	3.741
7-H	1.955(11)	1.921(13)	1.991(9) 2.088(9)	80.9(5)	91.7(3)	3.350
7-Me	1.996(3)	1.969(3)	2.002(2) 2.079(2)	81.65(12)	92.10(10)	4.605
7-OMe	1.991(3)	1.968(3)	2.003(3) 2.082(3)	81.57(15)	91.61(12)	3.240
9	1.995(4)	1.957(4)	2.001(3) 2.094(3)	81.56(17)	92.04(13)	3.394
11	1.987(13)	2.014(15)	1.998(10) 2.064(11)	80.5(6)	92.0(4)	4.953

character for **7-R** (vide infra). Complex **9** absorbs at a longer wavelength than that for [Pt(ppy)(acac)], and the introduction of an electron-donating diphenylamino group into the electron-deficient pyridine moiety of the ligand is expected to increase the donor−acceptor (D−A) character of the ligand, leading to a larger π-conjugation space and/or strong intramolecular D−A interaction. For **11**, a shoulder band at 421 nm with an extinction coefficient of 3000 M^{-1} cm^{-1} is also observed as a result of the concomitant observation of the metal-to-ligand CT (MLCT) transition. This can be corroborated with the computational results in which the valence orbital picture consists of combined LC and MLCT components in the lowest energy absorption (vide infra). In contrast, the other Pt(II) complexes possess predominantly ³LC character in the excited state.

Both **6-R** and **7-R** are good light emitters in fluid solutions and in the solid state at 298 K. Each of the luminescence spectra of **6-R** is dominated by LC ¹($\pi-\pi$*) transitions in the visible region, and the emissions vary from 462 to 537 nm (Figure 3a). For **6-R**, the emissions are sensitive to

Table 3. Photophysical Data for the New Pt Complexes and Their Ligands

compound	T_{decomp} (°C)	λ_{max} (nm)[a]	λ_{em} (nm)[b]		
			CH$_2$Cl$_2$ (298 K)	Φ (%)	frozen CH$_2$Cl$_2$ (77 K)
6-F	466	293 (5.4), 364 (6.7)	462 (3.8)[c]	81	
6-H	456	294 (6.5), 368 (7.1)	470 (4.2)[c]	70	
6-Me	466	296 (5.0), 375 (5.2)	499 (4.6)[c]	57	
6-OMe	421	294 (2.2), 375 (2.2)	537 (2.7)[c]	40	
8	341	347 (2.2)	429 (3.1)[c]	89	
10	358	307 (1.8)	341*, 357 (6.4),[c] 373*	98	
ppy		222 (1.0), 248 (1.2), 276 (0.9)	333*, 349 (0.13)[c]	2.0	
7-F	304	293 (5.1), 370 (4.9)	429* (3.0),[c] 533 (3.1),[d] 573*	3.0	537 (6.2),[d] 582*, 625*
7-H	370	294 (8.0), 372 (7.5)	471 (2.8),[c] 533 (7.0),[d] 570*	2.2	538 (7.2),[d] 582*, 625*
7-Me	341	295 (5.3), 381 (4.5)	496* (3.1),[c] 534 (5.4),[d] 571*	1.7	536 (6.4),[d] 583*, 625*
7-OMe	255	294 (1.5), 385 (1.3)	468* (2.2),[c] 534 (3.1),[d] 572*	0.7	537 (3.1),[d] 583*, 626*
9	316	307 (1.7), 337 (1.5), 421 (1.6)	479 (2.7),[c] 535 (4.1)[d]	0.5	537 (4.7),[d] 579*
11	350	322 (3.2), 341 (2.9), 421* (0.3)	422* (2.1),[c] 533 (4.9),[d] 573*	0.5	538 (5.0),[d] 579
[Pt(ppy)(acac)]	294	250 (3.2), 277 (2.2), 313 (1.1), 325 (1.0), 360 (0.6), 392* (0.4)	481 (2.0)[d,e]	2.1[e]	478 (5.3), 495*, 505*, 516*, 548*[e]

[a] Extinction coefficients (10^4 M^{-1} cm^{-1}) are shown in parentheses. [b] Asterisks indicate emission peaks appearing as shoulders or weak bands. [c] Fluorescence lifetimes (ns) shown in parentheses are measured in CH$_2$Cl$_2$. [d] Phosphorescence lifetimes (μs) shown in parentheses are measured in CH$_2$Cl$_2$. [e] Data measured in 2-methyltetrahydrofuran can be taken from ref 24a.
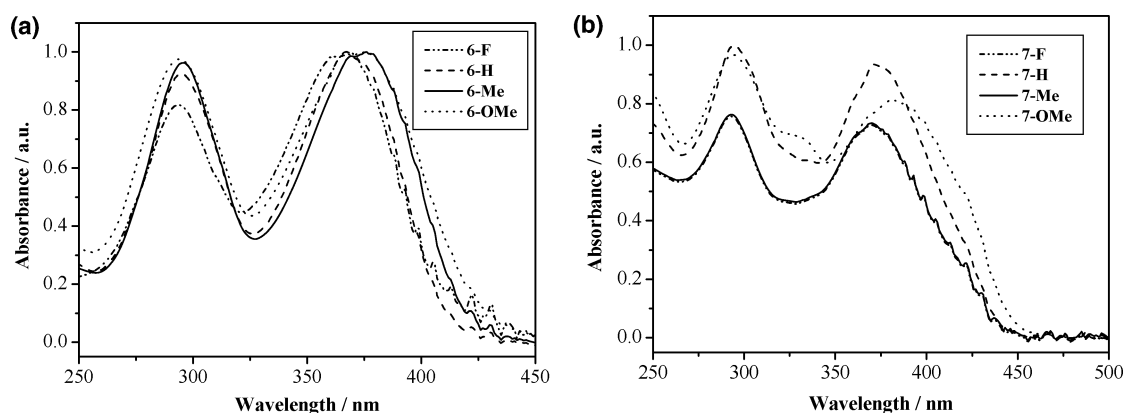
Figure 2. Absorption spectra in CH$_2$Cl$_2$ at 298 K for (a) **6-R** and (b) **7-R**.

the para substituents and the emission wavelength is affected by the electronic properties of R in the order OMe > Me > H > F. In other words, compound **6-F**, which contains electron-withdrawing fluoro-substituted triphenylamine, shows an ipsochromic-shifted emission ($\Delta\lambda = 8$ nm), while those containing electron-releasing substituents (Me and OMe) undergo a large bathochromic-shifted emission ($\Delta\lambda = 29$ and 67 nm for the Me and OMe cases) with respect to the unsubstituted ligand **6-H**. Hence, it can be inferred that the position occupied by the substituents in the amine group is dominated by HOMO character. These results also indicate that the electron-donating and -accepting moieties can raise and lower the HOMO levels, respectively. For **7-R**, each of them shows dual emission peaks (viz., fluorescence and phosphorescence) at 298 K (Figure 3b). Upon introduction of both triarylamino and oxadiazole functional groups into the phenylpyridine ligands, the Pt(II) center should show a reduced spin−orbit interaction. As a result, both LC fluorescence and phosphorescence can be observed.[9f] The large Stokes shift, the structured luminescence, and microsecond radiative decay lifetimes for the low-lying bands are in line with emission arising from a LC $^3(\pi−\pi*)$ excited state in **7-R**.[24] The vibronic splitting at ca. 1407−1506 cm^{-1} (ν_{0-1}) in the emission profile corresponds to the aromatic stretching modes of the ligands, which is diagnostic of the involvement

of the intraligand $\pi−\pi*$ transitions in the emission, and these vibronic fine structures preclude the assignment of ^{3}MLCT states, which are usually broad and featureless. Consistent with the X-ray structural data, examination of the emission behavior of **7-R** (except for **7-Me**) in CH$_2$Cl$_2$ and in the solid state suggests the presence of solid-state aggregates in thin neat films.[29] Figure 3c depicts the solid-state PL spectra for three of them, which indicate the existence of an aggregate emission band at 650 and 653 nm for **7-H** and **7-OMe**, respectively, but it is absent for **7-Me**. As is evident from the absence of Pt···Pt short contacts in the crystal state, complex **7-Me** is less prone to aggregation and the emission solely arises from the triplet exciton in the solid phase. While the higher-lying fluorescent emission was found to show a red shift in the wavelength along the series **7-F** → **7-H** → **7-Me** → **7-OMe**, attachment of different R groups does not seem to alter the phosphorescent emission energies of these complexes. Presumably, the singlet state may be described as a zwitterion, and so the inductive effect is consistent with the shift observed. For the phosphorescence, the triplet state is better described as a diradical, and so the inductive effect is much less felt and not much shifting would be anticipated.[30] Also, by looking at the fluorescence band, we see

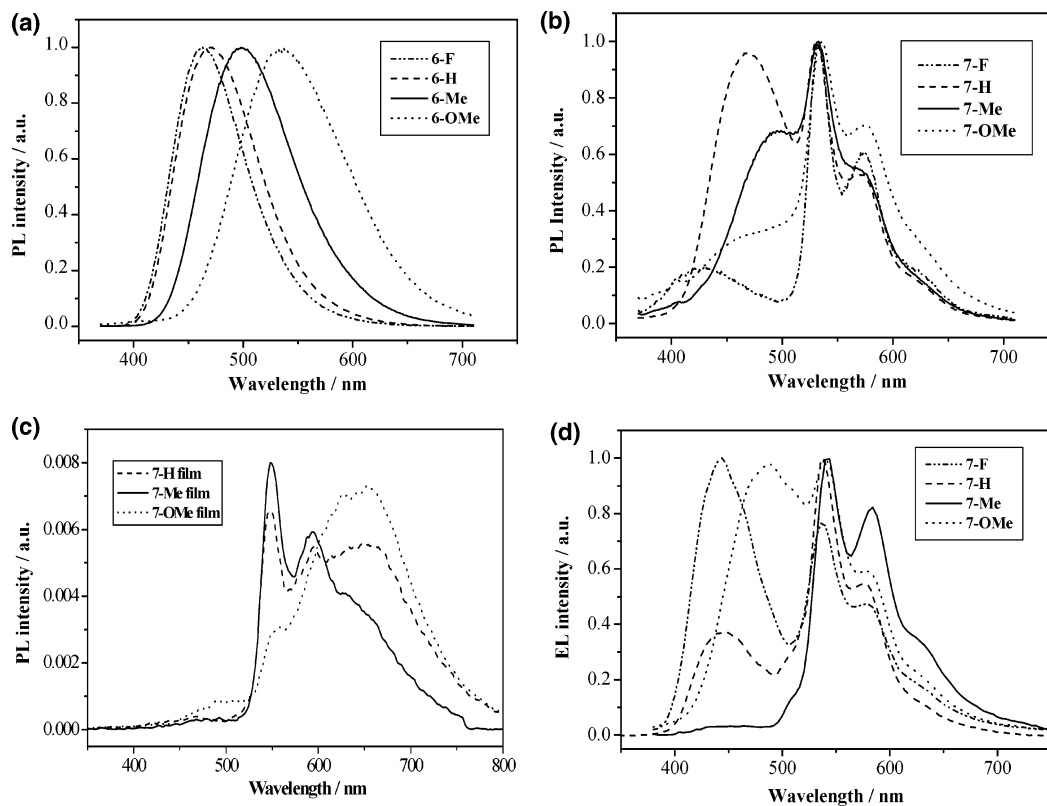(29) Bunz, U. H. F. *Chem. Rev.* **2000**, *100*, 1605−1644 and references cited therein.

Figure 3. Solution PL spectra of (a) **6-R** and (b) **7-R** in CH$_2$Cl$_2$ at 298 K. (c) Neat thin-film PL spectra of **7-R** (R = H, Me, OMe). (d) EL spectra of OLED devices **I−IV** at the 5 wt % dopant level of **7** at 8 V.

no vibronic structure, while phosphorescence has some. This tells us that there may be a twist CT phenomenon, where a twist angle changes very much in the singlet state.[31] Low-temperature emission spectra were also recorded for the new Pt(II) complexes at 77 K, and they essentially become dominated by the intense phosphorescence bands in frozen CH$_2$Cl$_2$ at the expense of the fluorescence peaks. The phosphorescence lifetimes at 77 K are longer than those at room temperature. The small quantum yields of these complexes indicate that the emission lifetimes of the Pt(II) complexes are determined by nonradiative decay rates, which usually decrease with lowering temperature. Thus, a lengthening of the lifetime at low temperature would be anticipated.

DFT Calculations. Molecular orbital calculations at the B3LYP level of DFT were performed on the two series of compounds **6-R** and **7-R** to study their electronic structures. For **6-R**, the HOMO mainly consists of an out-of-phase combination between the π orbitals of the three N(amine)-bonded phenyl rings and the amine−N p$_\pi$ orbital, while the LUMO is derived from the π* orbitals of the oxadiazole ring and the phenylpyridyl group. For **7-R**, HOMO and LUMO are similar to the corresponding **6-R** except that the orbitals are slightly more localized. In addition, contribution of the metal orbitals can be found in the HOMO−1 and LUMO of **7-R**. The DFT results indicate that the feature of the frontier molecular orbitals does not change significantly

with different substituents. As an example, Figure 4 shows four frontier molecular orbitals for **6-F** and **7-F**. The calculated HOMO−LUMO gaps for **6-R** follow the order **6-OMe** (3.27 eV) < **6-Me** (3.37 eV) < **6-H** (3.55 eV) < **6-F** (3.82 eV). The trend is expected because the highly electronegative F substituents tend to stabilize the HOMO significantly, giving the largest energy gap, while the strongly electron-donating OMe groups give the smallest gap. As expected, the HOMO−LUMO gaps become smaller with the presence of a metal fragment because metalation of **6-R** makes **7-R** "electron-richer". Like **6-R**, the calculated order of HOMO−LUMO gaps for **7-R** is **7-OMe** (2.99 eV) < **7-Me** (3.22 eV) < **7-H** (3.46 eV) < **7-F** (3.47 eV).

For **6-R** and **7-R**, it was shown that the NAr$_2$ groups govern the feature of the HOMOs. We also examined the molecular orbitals for the model compounds **10** and **11** without the NAr$_2$ units. Figure 5 contains the relevant frontier molecular orbitals for **7-H** and **11**. The LUMO for **11** is similar to that for **10**, corresponding to the lowest π* orbital extensively delocalized on the oxadiazole-containing ligand. The HOMO for **10** is derived from the orbitals of the phenylpyridine unit and the oxadiazole ring. For **11**, however, the HOMO is derived mainly from the orbitals of the inner phenyl ring of the organic ligand and the metal−acac fragment with a substantial amount of metal character. The theoretical HOMO−LUMO gaps of 4.51 eV for **10** and 3.79 eV for **11** are clearly greater than those calculated for **6-H** and **7-H**, respectively, indicating that these non-amine compounds are relatively "electron-poor". Again, we see that

(30) Turro, N. J. *Modern Molecular Photochemistry*; University Science Books: Mill Valley, CA, 1991.
(31) (a) Harvey, P. D.; Durocher, G. *J. Photochem. Photobiol.* **1984**, *27*, 29−39. (b) Harvey, P. D.; Durocher, G. *Can. J. Spectrosc.* **1984**, *29*, 84−86.
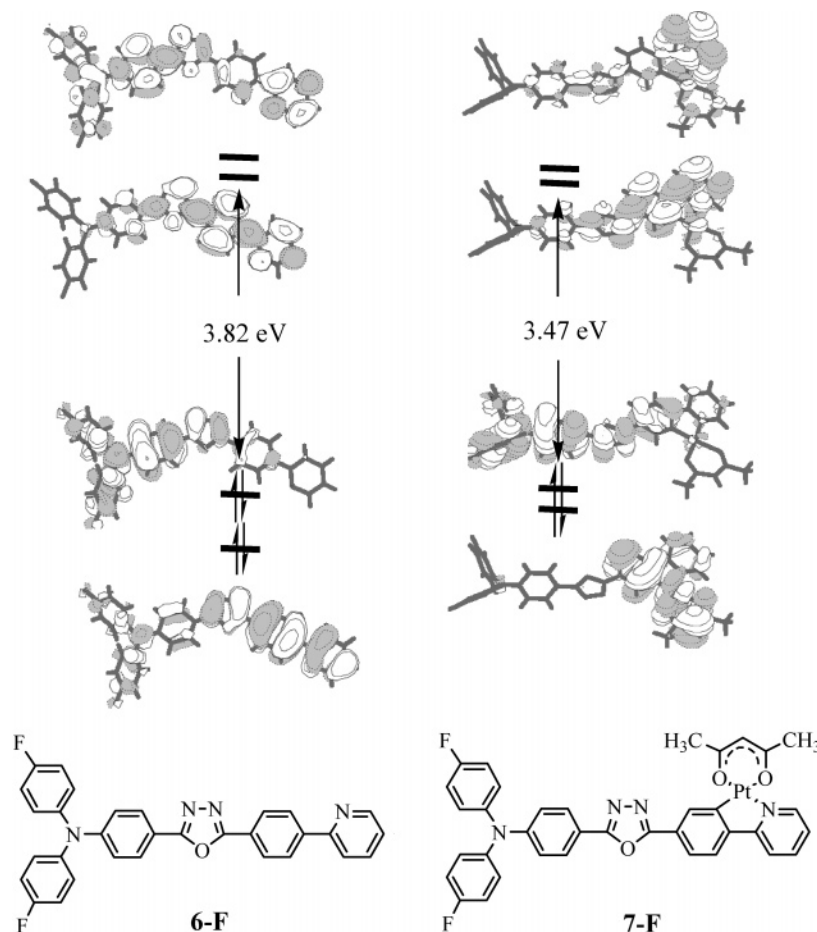
Figure 4. Contour plots of the frontier molecular orbitals for **6-F** and **7-F**.

the presence of the metal fragment reduces the HOMO−LUMO gap in **11** relative to **10**.

For **8** and **9**, which do not have an oxadiazole unit, the HOMOs of the two compounds are again mainly related to an out-of-phase combination between the π orbitals of the three N(amine)-bonded phenyl rings and the amine−N p orbital while the LUMOs are derived mainly from π^* orbitals of the pyridyl ring. The metal d orbitals contribute slightly to the HOMO−1 and LUMO of **9**. The calculated HOMO−LUMO gap for **8** (3.97 eV) is smaller than that for **10**, as a result of the fact that the oxadiazole unit is electron-withdrawing in nature. The gap calculated for **9** is less than that for **7-H**, suggesting that the neat NPh$_2$ entity can render **9** more electron-rich relative to the latter one containing an electron-deficient oxadiazole bridge. The gap calculated for **9** is smaller than that calculated for **8**, showing a similar metalation effect.

Redox Behavior. To investigate the electronic effects caused by the addition of R groups, cyclic voltammetry experiments were carried out for all complexes, including the ligand precursors. Because of the limited range available in CH$_2$Cl$_2$ and the inability of our instrument to measure the reduction potentials in the range from −2.7 to −3.5 V, we obtained only the oxidation potentials for our compounds (Table 4). The ligand redox properties are affected by cyclometalation, and complex **7-R** is easier to oxidize than **6-R** for each R. Reversible oxidation waves in the ranges of

0.37−0.76 V (for **6-R**) and 0.25−0.70 V (for **7-R**) that can be assigned to the oxidation of the triphenylamine moiety were observed. It is noteworthy that both series of complexes **6-R** and **7-R** reveal a gentle decrease in the oxidative potentials in the sequence F > H > Me > OMe, which is a manifestation of the inductive effect induced by the R substituents (viz., negative effect for F and positive effect for both Me and OMe). When **7-H** and **9** are compared, it is clear that the NPh$_2$ moiety in **9** tends to oxidize more easily than the one in **7-H** with the electron-withdrawing oxadiazole ring. This is also the case for the pure organic species **6-H** and **8**. However, the purely oxadiazole-containing counterpart **11** reveals a high oxidation potential at 0.89 V that appears harder to be oxidized compared to **7-H** having the electron-rich Ph$_2$N unit anchored to the oxadiazole ring. Notably, addition of electron-pushing NAr$_2$ groups to the ligand core in **11** caused a negative shift in the anodic half-wave potential by 0.19−0.64 V for **7-R**, with the largest shift observed for R = OMe. On the basis of the redox data, the HOMO levels can be estimated by taking −4.8 eV as the HOMO level for the Fc/Fc$^+$ couple with respect to the vacuum level.[32] The HOMO energies, together with the absorption edge data, were then used to compute the LUMO energy levels, and the results are also summarized in Table 4. The HOMO energies (from −5.05 to −5.50 eV) can be tuned easily by

(32) Thelakkat, M.; Schmidt, H.-W. *Adv. Mater.* **1998**, *10*, 219−223.
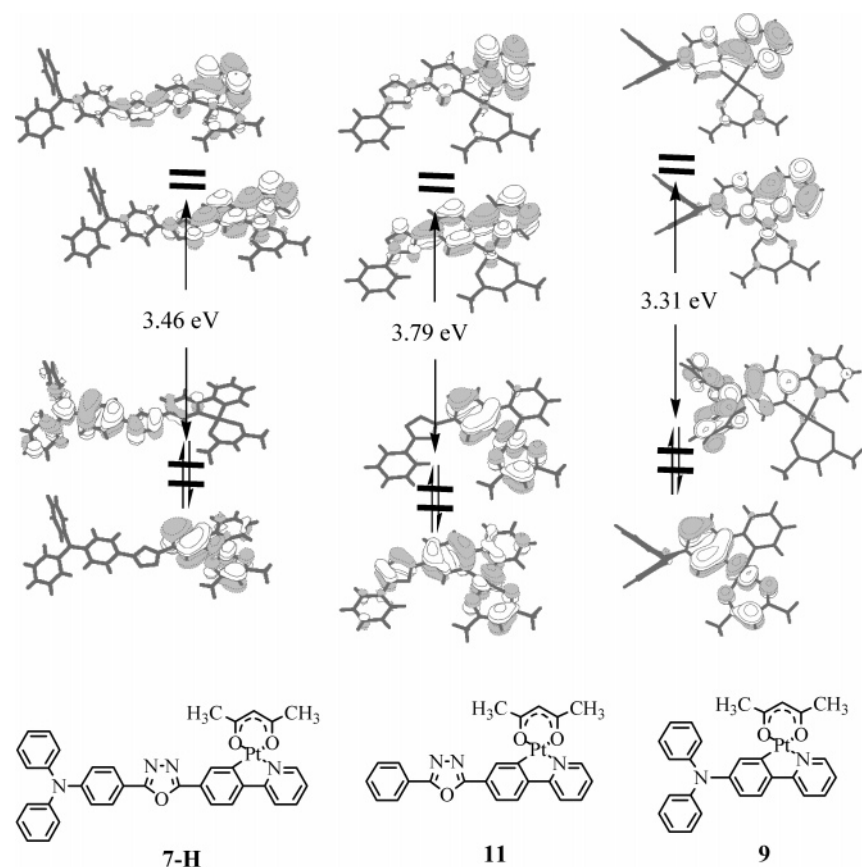
	7-H	**9**	**11**	**[Pt(ppy)(acac)]**
LUMO (eV)	−1.69	−1.40	−1.83	−1.60
HOMO (eV)	−5.15	−4.71	−5.62	−5.41

Figure 5. Contour plots of the frontier molecular orbitals for **7-H**, **9**, and **11**. The inset shows the DFT-calculated HOMO and LUMO levels for comparison, and the data for [Pt(ppy)(acac)] were taken from ref 24a.

Table 4. Electrochemical Properties and Frontier Orbital Energy Levels for **6−11**

complex	E_g (eV)	$E_{1/2}^{ox}$ (V)[a]	HOMO (eV)[b]	LUMO (eV)[c]	T_1 (eV)[d]
6-F	3.00	+0.76	−5.56	−2.56	
6-H	2.99	+0.66	−5.47	−2.48	
6-Me	2.95	+0.54	−5.34	−2.39	
6-OMe	2.90	+0.37, +0.98 (i)	−5.17	−2.27	
8	3.25	+0.46	−5.26	−2.01	
10	3.59				
7-F	2.73	+0.70	−5.50	−2.77	2.31
7-H	2.70	+0.66	−5.42	−2.72	2.30
7-Me	2.65	+0.49	−5.29	−2.64	2.31
7-OMe	2.57	+0.25, +0.85 (i)	−5.05	−2.48	2.31
9	2.64	+0.29, +0.83	−5.09	−2.45	2.31
11	2.95	+0.89	−5.69	−2.74	2.31
[Pt(ppy)(acac)]	2.93	e	e	−2.41[f]	2.59

[a] 0.1 M [Bu$_4$N]PF$_6$ in CH$_2$Cl$_2$ vs a Fc/Fc$^+$ couple. [b] The HOMO level was calculated by using the Fc value of 4.8 eV below the vacuum level. [c] Estimated from the HOMO and band-gap energies (LUMO = E_g + HOMO). [d] Determined from the PL spectrum in CH$_2$Cl$_2$ glass at 77 K. [e] Not reported. [f] The value was taken from ref 24. i = irreversible.

attaching various R groups to the aryl rings. The HOMO levels for **7-R** match closely with the energy levels for 4,4′-bis[*N*-(1-naphthyl)-*N*-phenylamino]biphenyl (NPB; HOMO = −5.20 eV)[33] and especially for **7-Me**; its promising

HOMO level of −5.29 eV is expected to facilitate transport of holes efficiently for achieving the best device performance among the four complexes (vide infra). When the diaryl-amino end groups are attached to the oxadiazole rings in **11**, the HOMO values of **7-R** are raised by as much as 0.64 eV for **7-OMe** and the HOMO of **7-OMe** is close to that for **9**. The elevated HOMO energy levels for **7-R** as compared to those for **11** (−5.69 eV) indicate that **7-R** compounds are more electropositive (or have lower ionization potentials) than the non-NPh$_2$-capped analogue **11**, and a better HT character in **7-R** can be expected. The LUMO levels of **7-R** (from −2.48 to −2.77 eV) are lower than that of 2-(4-biphenylyl)-5-(4-*tert*-butylphenyl)-1,3,4-oxadiazole (PBD; −2.4 eV),[2c] one of the most widely used hole-blocking/ET materials, showing the good ET ability for **7-R**. Our data can be compared to the poorer ET property for the prototypical [Pt(ppy)(acac)] with a higher LUMO level of −2.41 eV.[24] Complexes **7-R** are thus anticipated to display intriguing bipolar character, akin to some organic EL

(33) (a) Xie, H. Z.; Liu, M. W.; Wang, O. Y.; Zhang, X. H.; Lee, C. S.; Hung, L. S.; Lee, S. T.; Teng, P. F.; Kwong, H. L.; Zheng, H.; Che, C. M. *Adv. Mater.* **2001**, *13*, 1245−1248. (b) Lee, S. T.; Wang, Y. M.; Hou, X. Y.; Tang, C. W. *Appl. Phys. Lett.* **1999**, *74*, 670−672.
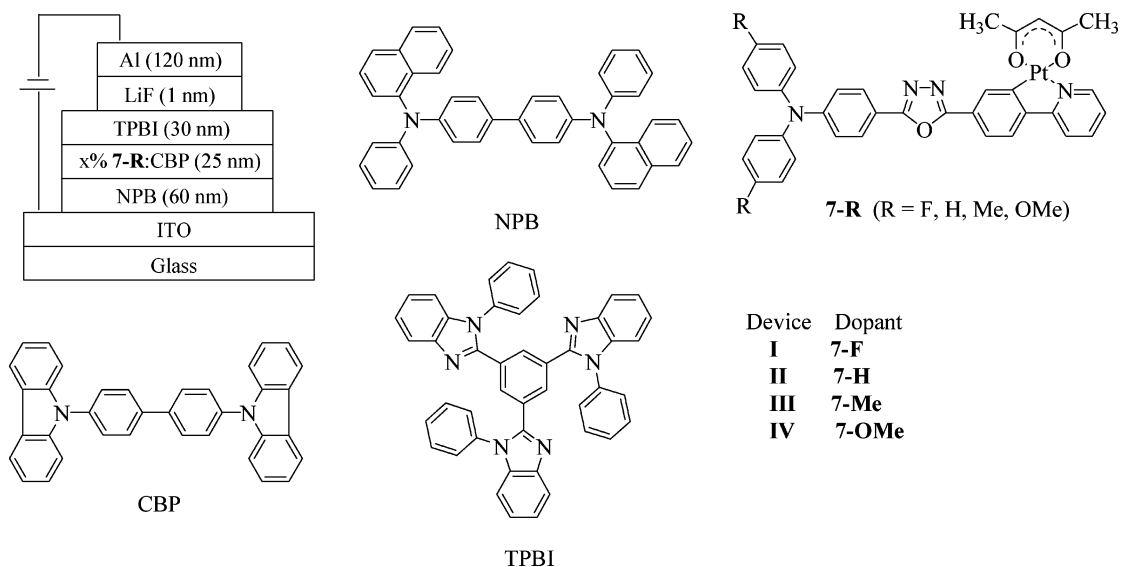
Figure 6. General structure for OLED devices and the molecular structures of the compounds used in these devices. TPBI: 2,2′,2″-(1,3,5-phenylene)-tris(1-phenyl-1*H*-benzimidazole). CBP: 4,4′-*N*,*N*′-dicarbazolebiphenyl. NPB: 4,4′-bis[*N*-(1-naphthyl)-*N*-phenylamino]biphenyl. ITO: indium−tin oxide.

materials.[6a] The LUMO levels are also compatible with that of 2,2′,2″-(1,3,5-phenylene)tris(1-phenyl-1*H*-benzimidazole) (TPBI; LUMO = −2.70 eV).[34] The electrochemical behavior here is in good agreement with a description of ligand-localized HOMO and LUMO states, as seen in our DFT calculations.

EL Devices and Substituent Effects. Organometallic phosphors **7-R** have very good film-forming properties for accessing their electrophosphorescent ability in evaporated devices. However, complexes **9** and **11** do not form good-quality films for electronic characterization in device structures. The good sublimability and short phosphorescence lifetimes of **7-R** [cf. >50 μs for Pt(OEP)][7b] render them suitable candidates as efficient electrophosphors. These phosphors are better used as a phosphorescent dopant rather than a single emission layer in OLEDs to prevent the severe self-quenching and formation of aggregates expected in the solid film. Taking the advantage that these cyclometalated Pt(II) complexes are neutral and are thermally stable, fabrication of OLEDs can be achieved in a guest−host system by vacuum deposition of such luminescent compounds. Figure 6 depicts the general four-layer structures for the electrophosphorescent devices and the molecular structures of the compounds employed. 4,4′-*N*,*N*′-Dicarbazolebiphenyl (CBP) acts as a small-molecule host material for the electrophosphor, NPB as a hole-transport layer, TBPI as both a hole-blocker and an electron-transporter, and LiF as an electron-injection layer. Here, TBPI, instead of the commonly used 2,9-dimethyl-4,7-diphenyl-1,10-phenanthroline or tris(8-hydroxyquinolinato)aluminum, was adopted for the devices to confine excitons within the emissive zone because it shows a higher electron mobility.[35] It is essential that the triplet level of the host be larger than that of the

triplet emitter to prevent reverse energy transfer from the guest back to the host and to effectively confine triplet excitons on guest molecules. Clearly, complexes **7-R** show triplet levels of 2.30−2.31 eV, well below the level of the CBP host (2.56 eV). The Pt(II) complexes were doped into the host material in the emitting zone with various doping contents for each sample. It is worth noting that, even at high current densities, emission from CBP is negligible in all cases, indicating complete energy and/or charge transfer from the host exciton to the phosphor molecule upon electrical excitation. Comparisons of the performances for the devices are summarized in Table 5. Figure 3d illustrates the EL spectra of the devices at the 5 wt % dopant level of **7-R** at a driving voltage of 8 V, and the impact of the aryl ring substituents with regards to the emission properties of this class of emitters is obvious. Generally, we observe both the electrogenerated fluorescence and phosphorescence bands. As expected, the electrofluorescence energy depends on the nature of R groups, but the electrophosphorescence energy is rather invariant of R, which is consistent with that observed for the PL in solution. There is no sign of metal complex aggregation in the fabricated devices **I−IV**. At the 5% doping level, the excited-state properties of **7-R** have been adjusted to yield blue-green (for **7-F**), green-yellow (for **7-H** and **7-Me**), and greenish-white (for **7-OMe**). For devices **II−IV**, the EL spectra exhibited no significant change with variation of the operating bias voltages from 6 to 12 V but the EL spectral pattern is dependent on the dopant concentration. In each case, the EL peak resembles that of its corresponding PL spectrum from a thin film, indicating that the same optical transition is responsible for light emission. As indicated below, the color of the EL can be tuned by a variation in the applied dc voltage as well as the dopant concentration.

Figure 7a shows the current density−voltage−luminance (*I*−*V*−*L*) curves of **7-Me**-doped OLEDs at four different doping concentrations. Essentially, each of the devices **IIIa−**

(34) Tao, Y. T.; Chuen, C. H.; Ko, C. W.; Peng, J. W. *Chem. Mater.* **2002**, *14*, 4256−4261.

(35) (a) Duan, J.-P.; Sun, P.-P.; Cheng, C.-H. *Adv. Mater.* **2003**, *15*, 224−228. (b) Chen, C. H.; Shi, J.; Tang, C. W. *Macromol. Symp.* **1997**, *125*, 1.

Table 5. Performance of Ir-Doped Electrophosphorescent OLEDs Recorded at 8 V

device	phosphor dopant	$V_{turn-on}$ (V)	L (cd m^{-2})	η_{ext} (%)	η_L (cd A^{-1})	η_p (lm W^{-1})	λ_{max} (nm)	CIE
Ia	5% **7-F**	3.5	4239 (13.0)[a]	1.93 (1.8)[a] 1.00[b]	3.58 (4.1)[a] 1.92[b]	2.81 (1.7)[a] 0.86[b]	443, 537, 578	(0.22, 0.20)
Ib	8% **7-F**	3.6	3256 (13.0)[a]	1.73 (2.8)[a] 0.88[b]	3.27 (4.1)[a] 1.92[b]	2.29 (2.7)[a] 0.87[b]	444, 537, 579	(0.25, 0.27)
Ic	10% **7-F**	3.7	1066 (13.0)[a]	1.01 (2.1)[a] 0.51[b]	1.11 (5.4)[a] 0.66[b]	0.83 (3.3)[a] 0.31[b]	445, 541, 582	(0.36, 0.42)
IIa	5% **7-H**	6.3	2250 (13.5)[a]	2.41 (1.6)[a] 1.32[b]	3.23 (1.7)[a] 2.09[b]	1.48 (0.5)[a] 0.73[b]	445, 538, 575	(0.30, 0.43)
IIb	10% **7-H**	6.0	3364 (13.2)[a]	1.93 (2.1)[a] 1.11[b]	4.89 (0.9)[a] 2.80[b]	2.56 (0.2)[a] 1.02[b]	445, 538, 578	(0.36, 0.54)
IIc	15% **7-H**	5.4	4055 (12.8)[a]	1.25 (2.4)[a] 0.74[b]	4.24 (1.2)[a] 2.81[b]	2.42 (0.2)[a] 1.11[b]	445, 538, 578	(0.37, 0.55)
IIIa	5% **7-Me**	4.7	2039 (11.0)[a]	3.59 (1.8)[a] 1.80[b]	10.95 (1.2)[a] 5.50[b]	5.73 (1.6)[a] 1.68[b]	542, 583	(0.44, 0.53)
IIIb	7% **7-Me**	4.7	1876 (11.0)[a]	2.72 (2.7)[a] 1.51[b]	8.20 (0.3)[a] 4.16[b]	4.87 (0.4)[a] 1.29[b]	450, 540, 584	(0.38, 0.44)
IIIc	10% **7-Me**	4.2	3269 (11.0)[a]	2.63 (1.4)[a] 1.17[b]	6.79 (1.6)[a] 3.00[b]	4.07 (2.0)[a] 1.08[b]	460, 540, 584	(0.33, 0.39)
IIId	12% **7-Me**	4.3	2495 (11.0)[a]	2.27 (3.0)[a] 1.28[b]	5.48 (3.4)[a] 3.07[b]	4.13 (0.5)[a] 1.20[b]	460, 540, 582	(0.30, 0.36)
IVa	2.5% **7-OMe**	5.1	8462 (20.1)[a]	2.30 (0.6)[a] 1.60[b]	5.50 (0.6)[a] 3.82[b]	2.50 (0.3)[a] 1.07[b]	468, 542	(0.25, 0.35)
IVb	5% **7-OMe**	5.6	4649 (18.1)[a]	1.10 (1.8)[a] 0.94[b]	2.90 (1.7)[a] 2.42[b]	1.30 (0.1)[a] 0.64[b]	487, 540	(0.27, 0.39)
IVc	7% **7-OMe**	9.4	2327 (20.1)[a]	0.61 (6.9)[a] 0.54[b]	1.50 (6.8)[a] 1.30[b]	0.30 (6.8)[a] 0.25[b]	490	(0.22, 0.36)

[a] Maximum values of the devices. Values in parentheses are the voltages at which they were obtained. [b] At 20 mA cm^{-2}.
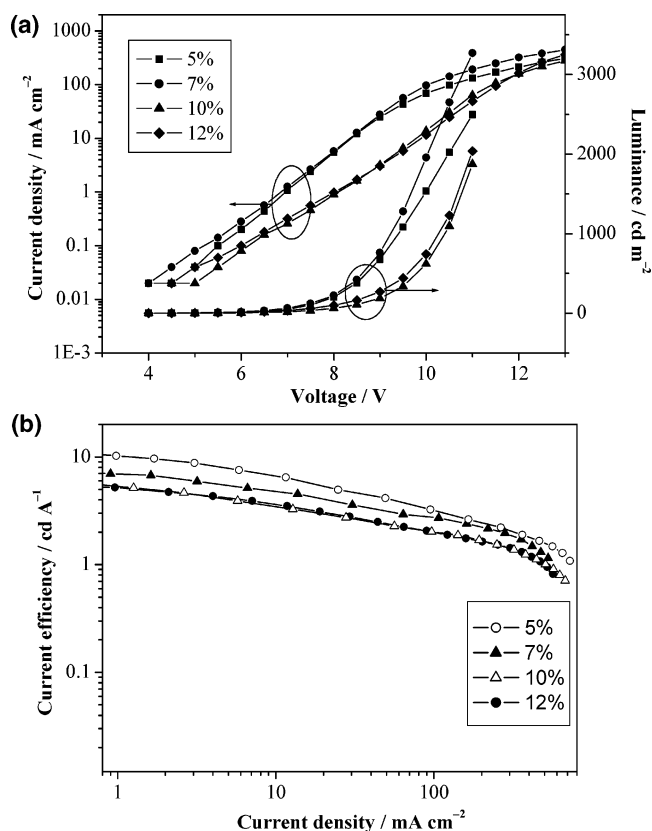

Figure 7. (a) $I-V-L$ characteristics of the electrophosphorescent devices **IIIa−IIId** with different dopant concentrations of **7-Me**. (b) Luminance efficiency as a function of the current density curve for devices **IIIa−IIId**.

IIId exhibits a prominent electrophosphorescence peak at about 540 nm with low turn-on voltages ($V_{turn-on}$) for light emission at 1 cd m^{-2} of 4.2−4.3 V. The luminance efficiency of the 5%-doped device **IIIa−IIId** as a function of the current density is presented in Figure 7b. The best perfor-

mance was realized in the green-yellow device **IIIa**, where a maximum external quantum efficiency (η_{ext}) of 3.59%, a luminance efficiency (η_L) of 10.95 cd A^{-1}, and a power efficiency (η_p) of 5.73 lm W^{-1} were obtained. For devices **IIa** and **IVb**, the EL spectra are dominated by two major emission bands and the corresponding peak efficiencies are η_{ext} = 2.41 and 1.10%, respectively. At a 2.5% ratio of **7-OMe** in device **IVa**, improved luminance (∼8460 cd m^{-2}) and efficiency (∼2.30%) are observed relative to device **IVb**. The higher efficiency and superior performance of **7-Me** over the others may be attributed to the better match of its HOMO level with NPB, which leads to excellent balancing of holes and electrons. At high concentrations beyond 5 wt %, η_{ext} tends to decrease slightly, apparently as a consequence of aggregate-induced quenching, and the maximum η_{ext} was achieved at 5 wt % concentration in most cases except for device **IV**, where the highest η_{ext} at the 2.5 wt % level was obtained. In common with most phosphorescent devices, there was a gradual decrease in efficiency with increasing current density, which has been attributed to a combination of triplet−triplet annihilation[36] and field-induced quenching effects.[37]

WOLEDs. To achieve the goal of white light emission, two strategies have been employed in this study using the multifunctional compounds **7-F** and **7-Me**. For device **Ic** with 10% **7-F**, a strong voltage dependence of the EL spectrum is observed, with the blue color intensity increasing relative to the orange component at increasing voltage, owing to the requirement for high-energy excitation of the blue-light emitter. Figure 8a shows the EL spectra of device **Ic** at

(36) Baldo, M. A.; Adachi, C.; Forrest, S. R. *Phys. Rev. B* **2000**, *62*, 10967−10977.
(37) Kalinowski, J.; Stampor, W.; Mezyk, J.; Cocchi, M.; Virgili, D.; Fattori, V.; Di Marco, P. *Phys. Rev. B* **2002**, *66*, 235321-1−235321-15.
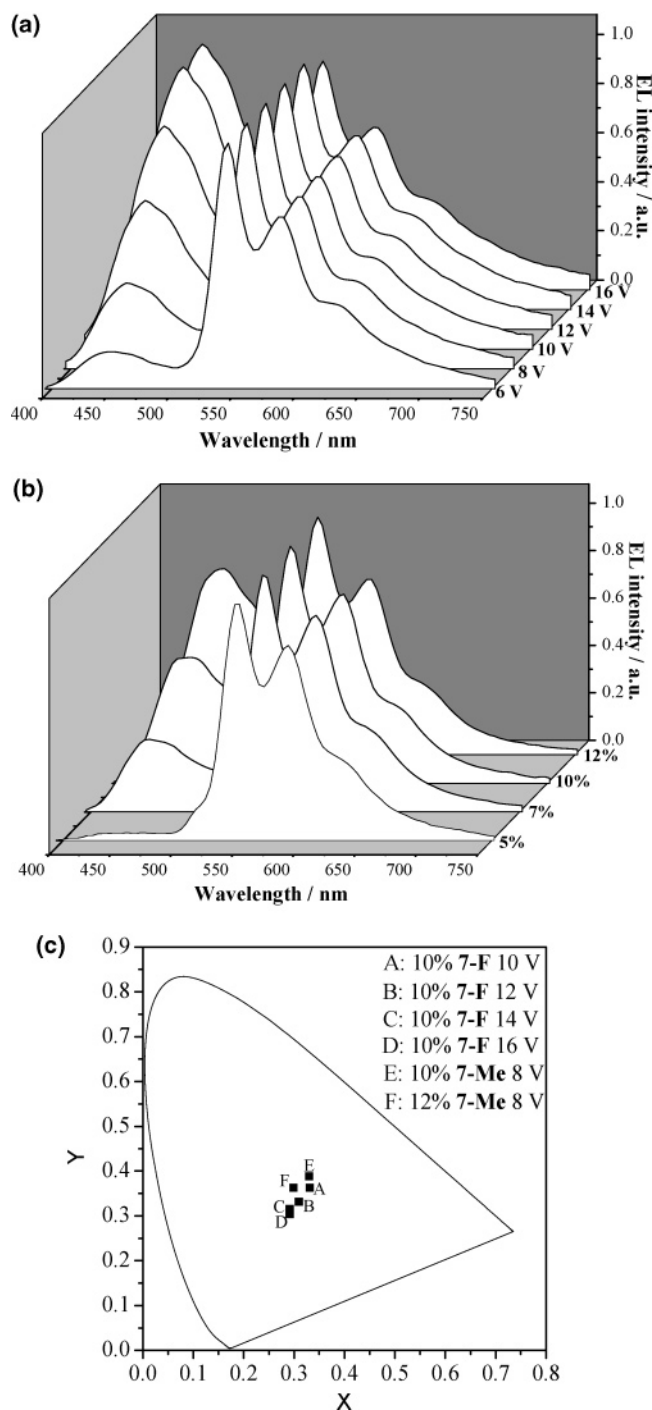
Figure 8. (a) EL spectra of **7-F**-doped device **Ic** at different dc voltages applied (from front to back: 6, 8, 10, 12, 14, and 16 V). (b) Devices **IIIa–IIId** with different concentrations of **7-Me** (5, 7, 10, and 12 wt %) as the dopant, upon applying 8 V of dc voltage. (c) CIE coordinates of white light sources.

Table 6. Performance Parameters of Various WOLEDs

device	voltage (V)	max η_{ext} (%)^a	CIE (x, y)
Ic	10	1.0 (2.1)	(0.33, 0.36)
Ic	12	1.0 (2.0)	(0.31, 0.33)
Ic	14	1.0 (1.9)	(0.29, 0.31)
Ic	16	1.0 (1.9)	(0.29, 0.30)
IIIc	8	2.6 (1.4)	(0.33, 0.39)
IIId	8	2.3 (3.0)	(0.30, 0.36)

^{a} Values in parentheses are the voltages at which they were obtained.

to almost white by applying different dc voltages from 10 to 16 V (Figure 8a and Table 6).

Additionally, to realize the generation of white EL that is not driven by varying the bias voltage, devices **IIIc** and **IIId** comprising 10 and 12 wt % of the dopant **7-Me** were prepared. Both devices begin to glow at ∼4.2 V and exhibit two emission bands at 460 and 540 nm in the EL spectra. The WOLED device **IIIc** gives peak η_{ext}, η_L, and η_P of 2.63%, 6.79 cd A^{-1}, and 4.07 lm W^{-1}, respectively. The highest achieved luminance is 3270 cd m^{-2} at 11 V. Saliently, the performances of both WOLED devices are slightly better than the previously reported results for Pt(II) Schiff base emitters (η_{ext} = 1.1% and η_P = 0.79 lm W^{-1}).[38] The Commission Internationale de L'Eclairage (CIE) coordinates of devices **IIIc** and **IIId** are (0.33, 0.39) and (0.30, 0.36), respectively (Figure 8c), which closely approach that of white light [defined as (0.33, 0.33)]; the near-white emission is produced by the simultaneous EL of both singlet and triplet excitons of the trifunctional molecules in the device. Upon an increase in the concentration of **7-Me**, it seems that the EL efficiencies are lowered gradually but the singlet emission of **7-Me** at ∼460 nm becomes more important in the EL spectra (Figure 8b); this is consistent with more efficient intermolecular quenching of triplet excitons at high dopant concentrations. As a consequence, the concentration-dependent color tuning can be accomplished by making use of the relationship between the singlet–triplet intensity ratio of the dual emission spectrum and the dopant concentration. Although the dependence of the EL color on the dopant level of other square-planar metal complexes has been reported, in which the EL spectra displayed both monomeric and excimeric emissions with different relative intensities upon variation of the dopant concentration,[10] the present work confers another platform for the tuning of OLED colors. While most examples of white phosphorescent OLEDs require dual or multiple dopants in multilayer devices, we note that a near-white EL has been achieved in this work using a single dopant configuration.

Conclusions

In conclusion, the present work reports the synthesis and characterization of some new light-emitting multifunctional cyclometalated complexes of Pt(II) incorporating both HT triarylamine and ET oxadiazole moieties, the study of their photophysical properties, single-crystal X-ray structural analyses, and their applications in monochromatic OLEDs.

different dc voltages applied. At a lower dc voltage (<6 V), the EL spectrum is essentially characterized by an orange vibronic-structured band at ∼541 nm. The EL spectra exhibit a blue broad band at ∼445 nm as the dc voltage is increased from 6 V. Upon increasing the bias voltage, the relative triplet–singlet intensity ratio of **7-F** decreases gradually at the expense of the orange triplet emission. Accordingly, the emission color of device **I** can be tuned from green-yellow

(38) Che, C.-M.; Chan, S.-C.; Xiang, H.-F.; Chan, M. C. W.; Liu, Y.; Wang, Y. *Chem. Commun.* **2004**, 1484−1485.

Phosphorescent Platinum(II) Complexes

Modification of the para substituents on the NAr$_2$ groups has been undertaken in order to facilitate the fine-tuning of the emission energy for the complexes and the HOMO−LUMO levels. End-capping of the [Pt(ppy)(acac)]-type molecules with a NAr$_2$ chromophore in the phosphor has been shown to offer advantages in terms of lowering the first ionization potential, which improves the HT properties. The color of the EL can be modulated by a variation in the applied dc voltage as well as by a change in the dopant concentration. These multicomponent systems have been demonstrated to be useful in accomplishing white light sources through variation of the dopant concentration and the driving voltage. Management of the relative EL intensities of the singlet and triplet excitons has been shown to be a good tool for making efficient single-dopant WOLEDs. These new triplet emitters have the potential for further optimization for tuning the emission closer to pure white by a judicious change in the composition.

Supporting Information Available: CIF data, synthetic procedures and spectroscopic data for **1-R−5-R**, EL spectra and *I*−*V*−*L* curves for devices **IIa-c** and **IVa-c**, and absorption and PL spectra for **9** and **11**. This material is available free of charge via the Internet at http://pubs.acs.org.

IC061566C